

Deposition of Ultrathin Films of Niobium Pentoxide onto n⁺-Si (111) Using Atomic Layer Deposition



WPI

A Major Qualifying Project (MQP) Report
Submitted to the Faculty of
WORCESTER POLYTECHNIC INSTITUTE
In partial fulfillment of the requirements
For the Degree of Bachelor of Science in

Chemical Engineering

By:
Antonio Ramirez

Project Advisors:
Professor Ronald Grimm
Professor Stephen Kmiotek

Date: April 2022

This report represents work of WPI undergraduate students submitted to the faculty as evidence of a degree requirement. WPI routinely publishes these reports on its website without editorial or peer review. For more information about the projects program at WPI, see <http://www.wpi.edu/Academics/Projects>.

Abstract

Ultra-thin niobium oxide on silicon is needed to form a passivation layer between the silanes and metallic silicon in silane linked perovskite – silicon solar cells. Atomic Layer Deposition (ALD) serves as a potential method of depositing thin films because of its extreme repeatability and general ease of use. Deposition of ALD films can be controlled by cycles, temperature, pressure, and substrate conditions. X-ray photoelectron spectroscopy and an overlayer model were used to determine film thickness on silicon wafers. Although an ideal set of parameters were not obtained, 20 cycle runs generally yielded consistent film thickness at a running flow rate of 5 sccm and a temperature of 150 °C. Issues with substrate contamination yielded problems with gaining consistent results. Future work will involve exploring more cycle counts and ways to mitigate contamination.

Table of Contents

1. Introduction	1
2. Background.....	3
2.1 General Photovoltaics and Solar Cells.....	3
2.1.1 Silicon Solar Cells	3
2.1.2 Perovskite Solar Cells	5
2.1.3 Silicon-Perovskite Solar Cells.....	7
2.2 Introduction to Thin Films	8
2.3 Characteristics of Thin Films.....	9
2.4 Atomic Layer Deposition.....	10
2.5 Characterizing Thin-Films Using X-ray Photon Spectroscopy	13
3. Experimental.....	16
3.1 Materials and Chemicals	16
3.2 Wafer Preparation	16
3.3 Atomic Layer Deposition.....	17
3.4 Synthesis of Niobium Oxide Thin Film on n ⁺ -Si.....	18
3.5 XPS	21
3.6 Overlayer Model Interpretation of Oxide Thickness	22
4. Results.....	28
4.1 XPS results.....	28
4.2 Overlayer Model Results	29
4.3 Pressure Results	33
4.4 Contamination Analysis	34
5. Discussion	36
6. Future directions	38
Appendix A: CasaXPS Peak Fitting Values.....	40
Appendix B: Mathematica Notebook	42
Appendix C: Raw Peak Areas from Experiments	44
Appendix D: Sample Notes	45
Appendix E: SOP for ALD	46
Bibliography	50

Table of Figures

Figure 2-1: Schematic of a solar panel, https://www.acs.org/content/acs/en/education/resources/highschool/chemmatters/past-issues/archive-2013-2014/how-a-solar-cell-works.html	4
Figure 2-2: Different Configurations of Silicon-Perovskite Solar Cells, Carl, A. Soft, Organic, Carrier-Selective Contacts at Inorganic Semiconductor Interfaces Enabled by Low-Defect Covalent Bonding. Ph.D. Dissertation, Worcester Polytechnic Institute, Worcester, MA, 2020.	6
Figure 2-3: Illustration of possible solution to passivation issue	8
Figure 2-4: Illustration of the ALD process, https://www.sciencedirect.com/science/article/pii/S1369702114001436	11
Figure 2-5: Diagram illustrating how X-rays produce photoelectrons, https://serc.carleton.edu/msu_nanotech/methods/xps.html	14
Figure 2-6: Schematic of a general XPS instrument, https://grimmgroup.net/research/xps/background/ .	15
Figure 3-1: Process flow diagram of the Atomic Layer Deposition (ALD) instrument.	17
Figure 3-2: The Simplest Substrate-Overlayer Model.	22
Figure 3-3: Niobium Pentoxide over-layer model	23
Figure 3-4: Silicon Cubic Unit Cell Modeled in VESTA	25
Figure 3-5: Niobium Pentoxide Unit Cell Modeled in VESTA	26
Figure 3-6: Theoretical Graph of the Silicon/Niobium Intensity Ratio vs the Thickness of Niobium Pentoxide.	27
Figure 4-1: Multiplex results from XPS. From A to E: O 1s, C 1s, Nb 3d, and Si 2p	28
Figure 4-2: Serial and Parallel exposure set-up of AR25-30	31
Figure 4-3: Pressure of Niobium vs Idle Running Pressure for 3 Separate Runs.	33
Figure 4-4: Pressure of Water vs Idle Running Pressure for 3 Separate Runs.	33
Figure 4-5: Carbon and Niobium Ratios for All Samples	34

Table of Tables

Table 3-1: ALD Temperatures at 3 states; Standby, Pregame, and Running.	19
Table 4-1: Data for Set 1 Involving 20 cycles at 150 °C	29
Table 4-2: Data for Set 2 Involving 20 cycles and 150 °C	30
Table 4-3: Data for set 3 Involving 30 cycles and 150 °C	30
Table 4-4: Data from Serial Exposure Runs in Set 4 Involving 20 cycles and 150 °C.	31
Table 4-5: Data from Parallel Exposure Runs in Set 4 Involving 20 cycles and 150 °C	32
Table 4-6: Data for other samples	32
Table 4-7: Data from AR-4, AR-16, and AR-23	34

1. Introduction

In 2019, the world consumed 173,000 terawatt hours of energy. 79% of that energy came from non-renewable sources such as oil, gas, and coal.¹ These so-called fossil fuels are only available in finite quantities and will be exhausted.² For example, it was estimated in 2013 that the Earth's supply of oil will last approximately 53 more years.³ Because fossil fuels are finite, it has become increasingly important to find renewable energy sources. Renewable energy comes from sources such as wind and solar. Such sources are considered infinite. Renewable energy sources have many benefits over their fossil fuel counterparts. The biggest advantage over fossil fuels is that renewable energy is far cleaner for our environment. Although renewable energy still has impacts on the environment, reduced water and land use, less air and water pollution, less wildlife loss, and little to no greenhouse emissions make renewable energy a cleaner form of energy in every sense. On top of environmental benefits, renewable energy creates jobs, are low cost to install, and makes energy systems more resilient.² Among the renewable energy sources at our disposal, solar energy has the most potential. The sun provides 173,000 terawatts of energy *continuously* to the earth's surface. The potential to harvest even a fraction of this energy will mean clean and renewable energy being received from a free source, the sun. Like most forms of renewable energy, solar is clean, cost effective, promotes energy independence, and creates economic growth.⁴

There are three main ways to harness the immense energy the sun gives us; photovoltaics, solar heating and cooling, and concentrating solar power. Photovoltaics (PV) produce energy directly from the sunlight via electronic processes. Solar heating and cooling (SHC) and concentrating solar power (CSP) both use the heat from the sun to provide heating for systems such as turbines. Solar can be utilized on the roofs of homes or in large scale solar plants.⁵ Solar cells are the most popular form of solar energy. Solar cells are a form of photovoltaic devices that harness the energy from the cell and convert it into usable electricity. Such cells boast similar advantages to all renewable energy sources. Despite the benefits of solar cell energy, there are some fundamental limitations on the physics of solar cells that limit the efficiency. The current solar cell market is dominated by single junction solar cells. Single junction solar cells

are cells that have one absorbing region for light. The main component in single junction cells is silicon. Silicon's many advantages in solar cells include being cheap and being one of the most well understood elements. However, the limitation with such solar cells is the maximum possible efficiency. The efficiency of a solar cell is how well it converts the solar energy it absorbs into useable energy. The calculated limit for a single junction, silicon solar cell is around 29%. To increase efficiency of cells, we can utilize tandem junction solar cells. Tandem junction cells create two areas for light to be absorbed. This is achieved by having materials with different absorbing regions in the same cell. Solar cells with three or more materials are also possible. The most efficient solar cell that has been created is a four-junction solar cell with an efficiency of 46%. The problem with many tandem junction cells is that they are significantly more expensive than single junction silicon cells. Recently, perovskite-silicon tandem solar cells have become a solid competitor to conventional Si cells.⁶

Alex Carl, a PhD student in Grimmgroup, spent much of his PHD working on such perovskite structures. Alex's thesis spends time discussing a large issue with perovskite solar cells. The issue is with the electron transport layer (ETL) and the contact with the silicon substrate surface. ETLs must passivate the surface to allow for little to no oxidation of the silicon substrate. If oxidation occurs, the efficiency of the solar cell will decrease. Current ETLs are mostly metal oxides. Current metal oxides used, such as TiO_2 and SnO_2 , can passivate the surface. However, deposition procedures and prolonged exposure to light eventually induces unwanted oxidative effects.⁷ A solution to the oxidation problems is to find ETLs that are more resilient to oxidative deficiencies. Niobium Pentoxide, Nb_2O_5 , is a promising material that has shown to limit oxidation as an ETL when combined with silane linkers. To further test Nb_2O_5 's ability to perform as an ETL and passivation layer, thin films must be produced. In this paper, I will explore the process of depositing Nb_2O_5 onto a silicon substrate using atomic layer deposition. I will be finding running conditions to yield consistent layering at different cycle lengths. My research will serve as a gateway to exploring perovskite-silicon tandem solar cells with Nb_2O_5 as the ETL. In the following chapter, I will dive further into general photovoltaics, perovskite solar cells, thin films, atomic layer deposition, and characterizing techniques. The background will serve to set the stage further into why my research is important to the future of solar energy.

2. Background

To further understand the importance of the research done in my paper, this chapter will dive deeper into topics mentioned in the introduction. Such includes how a solar cell works in more detail, further detail into what a perovskite-silicon tandem solar cells are and how they work, and what are thin films and what are their strengths and weaknesses. Atomic layer deposition (ALD) and how thin films are characterized will be discussed as well. The latter two topics will put the techniques discussed in the experimental section into context.

2.1 General Photovoltaics and Solar Cells

Photovoltaic devices are devices that generate electricity from the sun. Electricity is generated through electronic processes that occur naturally on different types of materials. These materials are called semiconductors. When the photons from sunlight strike the semiconductor surface, it ionizes the material and causes the electrons to break free of their bonds. The structure of the semiconductor causes the flow of the electrons to go in one direction, which creates a current.⁸

2.1.1 Silicon Solar Cells

Solar cells utilize photovoltaics to generate electricity from the sun. Solar cells are layered into solar panels, which are what we see on people's homes and in solar farms. A solar panel is made of a semiconducting cell, a metal frame, a glass casing unit, and the wiring required to transfer the current.⁹ Figure 2.1 illustrates a simple silicon solar panel.

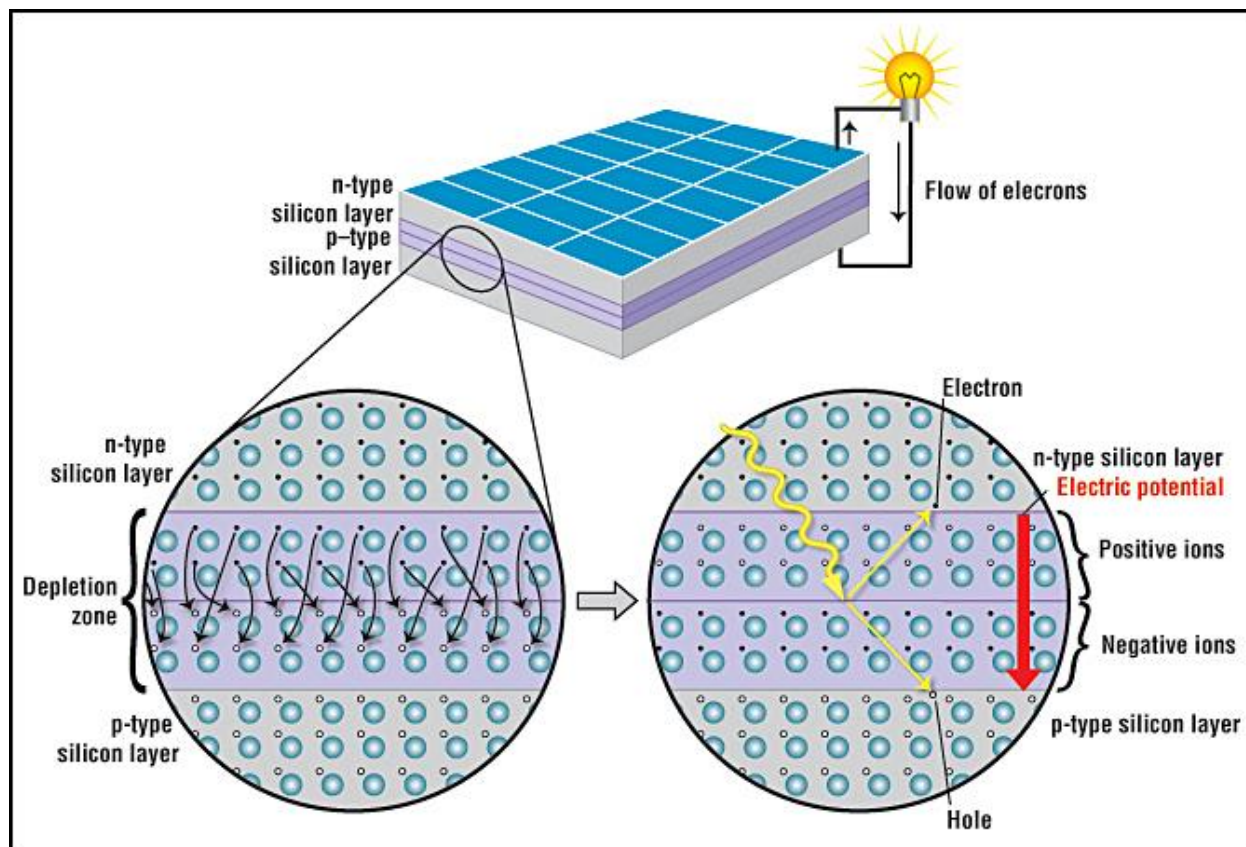


Figure 2-1: Schematic of a solar panel,

<https://www.acs.org/content/acs/en/education/resources/highschool/chemmatters/past-issues/archive-2013-2014/how-a-solar-cell-works.html>.

As seen in Fig. 2.1, a solar cell is made of two semiconductors, p-type and n-type silicon. P-type silicon is made by adding atoms to silicon that have less electrons in their outer shell than silicon. Examples of atoms that are commonly used in p-type silicon are boron and gallium. Boron, for example, has one less electron when forming bonds with silicon atoms. Because of the “missing” electron, an electron vacancy, known as a “hole” is formed. In contrast, n-type silicon is made with atoms that have one more electron in their outer shell compared to silicon. A common atom used in n-type silicon is phosphorus. Phosphorus has five outer electrons, but only 4 bonds with silicon. Because of such bonding, there is an extra electron free to move around the silicon structure. Solar cells are constructed with a layer of p-type silicon placed next to a layer of n-type silicon. At the interface of the two, electrons on the n-type side fill the “holes” on the p-type side. The area around the interface where the swapping takes place is called the depletion zone, as illustrated in Fig. 2.1. Once the holes are filled in the depletion zone, the p-type silicon side of the depletion zone is now negatively charged, and the n-type side is positively charged. The

oppositely charged ions creates an internal electric field. When the sunlight strikes the cell, electrons in the silicon are ejected. Such ejection forms holes. If holes are created in the electric field, electrons will move to the n-type layer, creating holes in the p-type layer. When connected with a conducting wire, electrons will travel from the n-type to the p-type, which creates a flow of electricity.¹⁰

The most important characteristic when it comes to solar cells is the cells efficiency. The efficiency can be defined by the amount of power coming out compared to the energy it absorbed. There are many properties of the solar cell that effect the efficiency. The most important property of the cell is the bandgap of the material the cell is made of. The bandgap of the material indicated what regions of light the material can absorb and convert to electricity. It is important to find bandgaps like the light that is being absorbed to maximize efficiency. As discussed earlier, silicon is the most common cell material due to its low cost and our large understanding of the element. Going further into the details, silicon cells have a crystalline structure. Such an organized lattice structure makes conversion to energy very efficient.¹⁰ Despite the advantages, the efficiency of silicon solar cells is reaching its limit. Such a limit is known as the Shockley-Queisser limit and is estimated to be at around 29%.⁶ Because of such a limit, it is important to find materials that can provide higher efficiencies.

2.1.2 Perovskite Solar Cells

Perovskite solar cells (PSCs) have gained popularity in the last decade due to their potential to have higher efficiencies than the Shockley-Queisser limit.⁷ A perovskite structure is a structure containing elements in the form ABX_3 .²⁵ More specific to solar cells, much research has gone into organic-inorganic metal halide perovskites.⁷ For example, early perovskites used in solar cells were methylammonium lead halides, which had the general form of $MAPbX_3$, where X is I, Br, or Cl. Perovskites of this nature yielded efficiencies around 14%. Current PSCs can yield efficiencies of 23-25%.⁶

Unlike silicon solar cells, PSCs do not contain the p-type – n-type junction to carry charge. Instead, they utilize carrier-selective transport. Carrier-selective materials conduct electrons and holes to be collected at their respective contact. The electrons and holes created by the sunlight are collected at opposite ends of the cell by carrier-selective materials. There are two types of carrier-selective materials, electron transport materials (ETM) and hole transport

materials (HTM). ETMs and HTMs can be organic or inorganic semiconductors and have energy levels capable of facilitating the flow of electrons and holes. In single junction PSCs, the ETM layer, or the electron transport layer (ETL), and the HTM layer, or the hole transport layer (HTL), can be in two different orientations. In a p-i-n cell, the light passes through the HTL, and in a n-i-p cell, light passes through the ETL first. The choice of what to use depends mostly on the materials of the layers and the stability in light. Figure 2.2 illustrates both p-i-n and n-i-p PSCs.

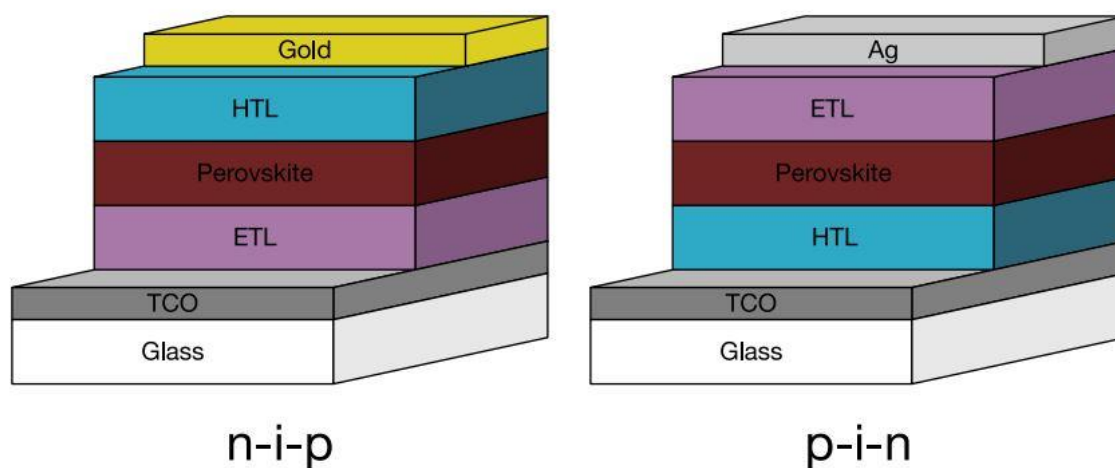


Figure 2-2: Different Configurations of Silicon-Perovskite Solar Cells, Carl, A. Soft, Organic, Carrier-Selective Contacts at Inorganic Semiconductor Interfaces Enabled by Low-Defect Covalent Bonding. Ph.D. Dissertation, Worcester Polytechnic Institute, Worcester, MA, 2020.

PSCs have properties such as a broad absorption spectrum, fast charge separation, and long carrier separation lifetimes.²⁴ Such properties allow perovskites to produce highly efficient, cheap, and flexible solar cells. Despite such advantages, one major disadvantage to perovskites is their stability. Instabilities in perovskite solar cells (PSC) are mainly due to inefficiencies with the ETL and the perovskite structure.²⁶ Therefore, finding ETL materials that have good efficiency with the perovskite is crucial in producing good PSCs. The most common ETL material is titanium dioxide (TiO_2), which boasts high resistivity and low electron mobility. Unfortunately, the efficiency of PSCs in single-junction are limited by the Shockley-Queisser limit as well.

2.1.3 Silicon-Perovskite Solar Cells

Because of the Shockley-Queisser limit, a need for more advanced solar cells is becoming more apparent. Current silicon solar cells are reaching 25% efficiency, which is getting close to the calculated 28% limit. Tandem junction solar cells can provide a solution to this problem. Tandem junction solar cells involve semiconductors stacked on each other. The stacking of semiconductors limits losses due to transmission and thermalization. Silicon-perovskite solar cells (Si-PSC) have many benefits over conventional silicon solar cells. Si-PSCs have the potential to have efficiencies over 40%. Perovskites and Silicon are also generally low cost, and silicon is one of the most well-known elements. The major downside of Si-PSCs is the optimization of the ETL. Such materials are very important to the performance of the solar cells. Popular ETMs for current Si-PSCs are TiO₂ and SnO₂. Such materials are usually deposited directly onto the silicon surface in thin films. If the ETL is not able to passivate the silicon surface, unwanted oxidation will severely decrease the efficiency of the Si-PSC. TiO₂ and SnO₂ can passivate the surface, but there are long term issues that cause oxidation regardless. Deposition procedures, high annealing temperatures, and prolonged exposure to light will induce oxidative defects over time. Because of such defects, there is a need for new and more efficient ETMs. Research is being done on both organic and metal-oxide ETLs, as well as combinations of the two. Rylene-based molecules, fullerenes combined with TiO₂, and long hydrocarbons such as C₆₀ are common organic ETLs.⁷ A metal-oxide that is being investigated as an ETM is niobium pentoxide (Nb₂O₅). Nb₂O₅ main benefit is its high stability. It also boasts a high band gap, which has the potential to improve the voltage of the cells. Figure 2.3 illustrates a possible solution to the oxidation problem.²⁶

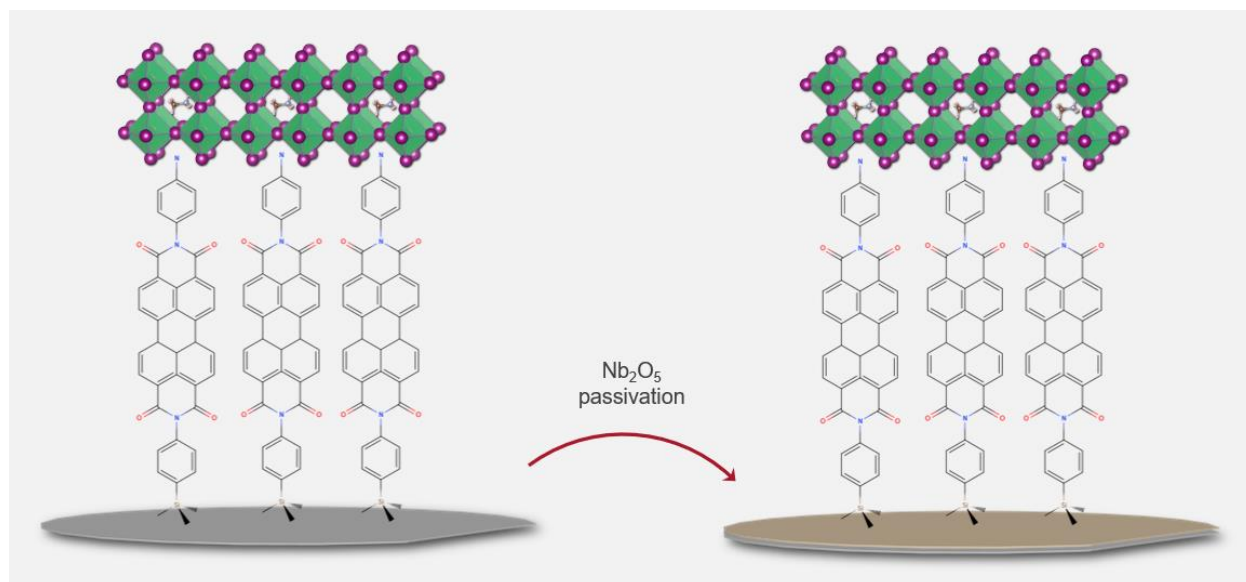


Figure 2-3: Illustration of possible solution to passivation issue

In Fig. 2.3, the perovskites are linked to the metallic silicon using a silane linker. In previous studies, the set up on the left has been used, but the interface between the organic silicon and metallic silicon has defects that decrease efficiency. Nb_2O_5 has the potential to passivate the metallic silicon as an ETM and decrease the defects.

To test Nb_2O_5 as a potential ETM, it must be produced in thin film in a controllable way. The main way to produce such thin films is through ALD. In the past, Nb_2O_5 thin films have been deposited using techniques such as sputtering.²⁷ However, to produce thin films that are usable as ETLs, more controlled techniques, such as ALD, are needed. To deposit Nb_2O_5 onto thin films, ALD precursor compounds are required. Due to the novelty of Nb_2O_5 deposition, not many precursors have been analyzed. The two major precursors that have been studied are *t*-BuN=Nb(NEt₂)₃ and *t*-BuN=Nb(NMeEt)₃. Both precursors have proven to produce high-quality ALD films with a variety of oxygen sources.²⁷ Further research on Nb_2O_5 thin films and its characteristics are needed to verify its potential, but preliminary research looks promising.

2.2 Introduction to Thin Films

Thin film coatings are vital to technology in the 21st century. Thin film technology is most prevalent today in the semiconductor and solar industries.¹³ Thin film is also used to produce reflective coatings on mirrors, CDs, sensors for chemicals, and many more.¹² Thin film deposition is the technology of applying a thin film of a compound to a substrate surface. There

are two main types of thin film deposition. The first form is called physical vapor deposition (PVD). Such a method is when the material is released from a source and deposited on a substrate using mostly mechanical processes.¹³ A common use of PVD is gold coating substrates using sputtering.¹³ The second form is called chemical vapor deposition (CVD). Such a deposition involves flowing a volatile precursor over a substrate. The precursor causes a chemical change on the surface of the substrate and leaves a chemically deposited coating.¹³ CVD is used in the semiconductor industry to produce high purity, high performance semiconductor materials.¹³ Thin film solar panels made using CVD have become increasingly more popular mainly due to the cheapness over conventional c-Si solar panels. The major downside to thin film solar cells is that they have historically been less efficient at collecting energy than c-Si. However, better compounds have been found for thin film solar cells and the efficiency of these solar cells has increased greatly.¹⁹

2.3 Characteristics of Thin Films

Thin film structure and properties can vary based on many different parameters. Such parameters include which technique was employed (PVD or CVD), substrate temperature, pressure of the system, and deposition rate. The structure of the film defines the properties of the film. There are 3 main types of thin film structures. Such structures can be defined as amorphous, polycrystalline, and epitaxial.¹⁴ Amorphous thin films contain structures that are of short order, meaning distances between crystals are comparable to interatomic distances.¹⁵ Growth of amorphous film takes place at low substrate temperatures and high deposition rates. Amorphous thin films are required for solar cells, transistors, and optoelectronics.¹⁴ Due to the small range order, amorphous films are difficult to study. However, they can possess qualities that make them useful for certain applications. For example, the lack of grain boundaries, or the interface between two crystals¹⁶, gives such films great mechanical properties.¹⁷ Polycrystalline films contain many nano and micro crystals. Such crystals are separated by grain boundaries.¹⁴ High temperatures are the main way to obtain polycrystalline films. Due to the different orientation of the crystals, the scattering of electrons can be controlled more readily. Because of such a feature, polycrystalline films are best used in applications such as thermoelectric.¹⁴ Finally, epitaxial films are like polycrystalline films, except the deposition of crystals is in a

nearly perfect lattice structure. Such films are mostly used in semiconductor applications due to their high quality.¹⁴

Electrical properties of thin films are key in determining the effectiveness in solar cells. When comparing the conductivity of the thin film with the conductivity of the bulk material, there are usually deviations.¹⁴ The reason for such deviations is largely attributed to a phenomenon known as the size effect. As the thickness of the bulk material is reduced, the distance over which an electron changes its direction or energy also reduces. Such a distance is known as the electron mean free path.¹⁸ The conductivity of a material generally decreases as the electron mean free path decreases.¹⁴ Therefore, as the thickness of the bulk material is decreased during deposition, the conductivity will also decrease. Such a relationship holds true for amorphous and crystalline films. Reductions in conductivity can also be due to specific structure defects, such as large grain boundaries that scatter electrons.¹⁴ Due to such scattering, the conductivity of polycrystalline films is much lower than an amorphous one. Other defects such as dangling bonds can trap electrons and prevent energy from being transferred.¹⁴

2.4 Atomic Layer Deposition

Atomic layer deposition (ALD) is a form of vapor deposition that involves sequential surface reactions onto a substrate, usually silicon.²⁰ Precursor chemicals, which usually contain the elements that are being deposited on the substrate, are introduced into the reaction chamber separately, with purge times in between.²⁰ The precursor leaves a monolayer of the chemical on the surface of the substrate. The precursors are introduced in cycles, making ALD a cyclic process, where other CVD techniques might have chemicals introduced continuously over long times.

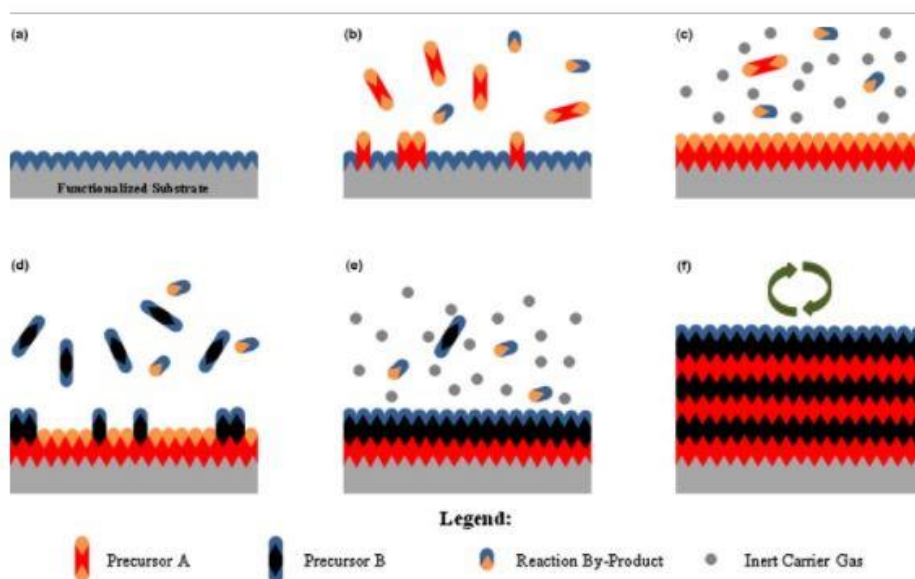


Figure 2-4: Illustration of the ALD process,

<https://www.sciencedirect.com/science/article/pii/S1369702114001436>

In Fig. 2.4, the ALD process can be seen in more detail. In 2.4b, precursor A is introduced to the system and reacts to the functionalized substrate surface, coating the surface in precursor A. In 2.4c, an inert gas such as argon is sent through the system, purging any unreacted precursor A and reaction side products out of the system. In 2.4d, precursor B is introduced to the system and allowed to react with the end of precursor A that is exposed. Finally, in 2.4e the system is purged again to rid the system of any remaining precursor B and reaction side products. 1f illustrates the cyclic nature of ALD, as 2.4b-2.4e can be repeated as many times as needed. Because of the cyclic nature, ALD enables very accurate film thickness.²¹ In ALD, film growth is generally only affected by precursor choice and process temperatures, meaning film growth can be easily characterized by simple parameters.

Advantages of ALD over other CVD techniques include extreme surface conformality, good repeatability, and general ease of scaleup.²⁰ ALD provides uniform thin films that are very good at conforming to the surface of the substrate. One example is the use of ALD to coat the trenches of semiconductor devices.²⁰ Going along with extreme surface conformality, ALD also provides pinhole-free coatings. Pinholes in thin film are small, circular areas where there is no growth.²² Such pinholes are caused by contamination on the substrate, such as dust. Pinholes can lead to decreased conductivity and efficiency. However, due to the nature of ALD deposition, films produced by ALD are pinhole free. ALD processes also have a high repeatability rate.

Because of such repeatability, ALD becomes an excellent way to optimize materials for coating solutions. Running ALD on a certain material can allow for ideal growth parameters to be found for that material. Once such parameters are found, they can be reliably used on different ALD machines, and scaled up with relative ease. Such scalability is especially important in industries such as solar. Testing on certain materials can be done in a small, lab scale ALD. When process parameters are found in the lab, they can be reliably scaled up to be able to produce large solar cells for use in solar panels.²⁰

All ALD processes include precursors. Such precursors contain the materials that are desired to be deposited onto the surface of the substrate. ALD precursors are unique when compared to other deposition methods because of the need for only surface reactions. Because of such uniqueness, many precursors used today have been specifically synthesized for ALD. ALD is a gas process, so precursors that are solid or liquid need to be stored in volatile conditions. Because of such volatile conditions, it is important that the precursors have good thermal stability over long periods of time.²⁰ In general, ALD precursors should follow the following guidelines:

1. Sufficiently volatile at deposition temperature
2. Able to absorb or react with substrate
3. Sufficiently reactive with another precursor
4. Reasonable priced
5. Able to be handled safely and preferable non-toxic

ALD precursors are generally non-metal or metal based, with each having their own advantages and disadvantages.

When looking at solar cells, a proper outer layer is needed to confine the generated charge from photons.²³ Such an outer layer is referred to as a surface passivation layer. The more efficient the surface passivation is, the more efficient the solar cell will be. ALD methods are very good at leaving pinole-free surfaces, which leads to great passivation properties.^{20,23} As mentioned earlier, thin-film solar cells have shown great improvement over conventional c-si solar cells. For example, CdTe thin film cells have an efficiency of 22%, a large increase over c-si cells. Unfortunately, Cd is very toxic, and Te is not a common element, so large scale production of such cells is not possible at the moment.²³ Other alternatives such as Sb₂S₃ and Cu₂SnS₃ films avoid the use of rare and toxic elements but have a lower efficiency. It is

theorized that nanoscale layer coating and interface modifications could provide improvements to the efficiency of films such as Sb_2S_3 and Cu_2SnS_3 . ALD techniques can provide nanoscale engineering through its self-limiting surface reactions. ALD can also provide ultrathin, dense, and continuous layers at nanoscales.²³ Because of such properties, ALD has become increasingly popular in the field of thin film solar cells.

2.5 Characterizing Thin-Films Using X-ray Photon Spectroscopy

Characterization of thin films is often done using spectroscopic techniques. Such techniques can give an insight into what elements are present on the surface. Coupled with mathematical models, spectroscopic data can also give data such as film thickness. X-ray Photon Spectroscopy is one of the oldest and most reliable forms of gaining surface characteristics from films.²⁸ XPS works because of the photoelectric effect. Such an effect describes the way electrons react when interacting with electromagnetic radiation.²⁹ When an electron is hit with radiation, a photoelectron is produced with an energy that can be described by the eq 2.1.²⁹

$$KE = h\nu - BE - \Phi \quad (2.1)$$

In eq 2.1, KE is the kinetic energy of the emitted photoelectron, $h\nu$ is the energy of the incident X-ray and is generally a fixed value based on the machine being used, BE is the binding energy of a given electron, and Φ is the work function, which is defined as the energy difference between the vacuum energy and the Fermi level.²⁹ The kinetic energy of the photoelectron depends on the binding energy of the electron. Because atoms have different orbitals at different energy states, there will be a range of emitted energies which will produce an XPS spectrum.²⁹ Figure 2.5 illustrates how the X-rays interact with electrons in the sample.

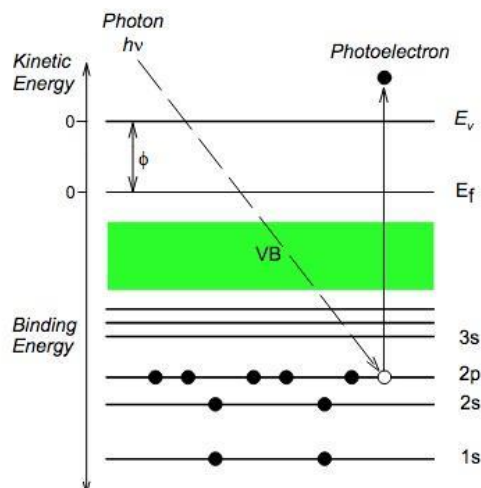


Figure 2-5: Diagram illustrating how X-rays produce photoelectrons,

https://serc.carleton.edu/msu_nanotech/methods/xps.html

XPS instruments are operated under ultrahigh vacuum, usually at less than 10^{-8} torr. Such a vacuum is required because photoelectrons are readily absorbed by the ambient atmosphere.²⁹ The X-ray source is usually Al $K\alpha$ or Mg α X-rays. A monochromator is used to assure that the only source X-rays strike the sample. A Concentric Hemispherical Analyzer (CHA) is most used to sort the energies of the photoelectrons that are emitted from the sample. Figure 2.6 illustrates the instrumentation of a general XPS device.²⁸

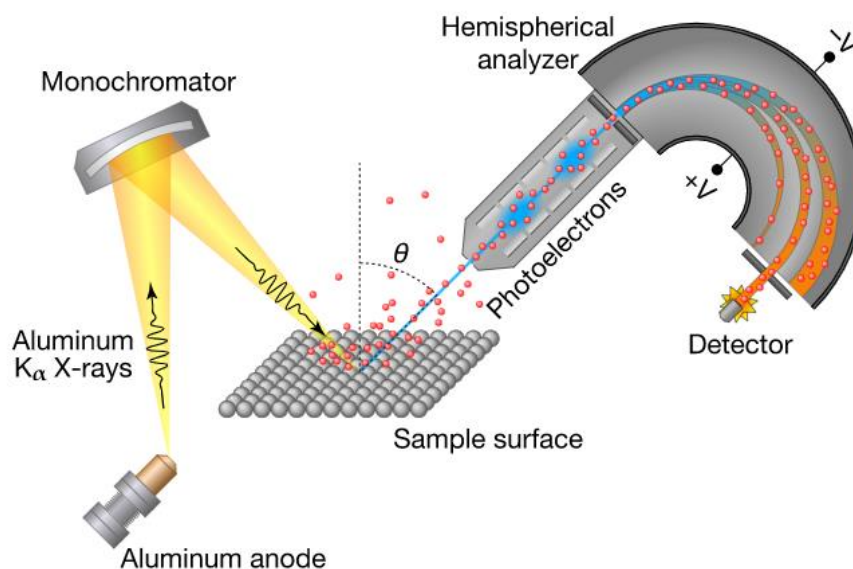


Figure 2-6: Schematic of a general XPS instrument,
<https://grimmgroup.net/research/xps/background/>

XPS has several advantages over other spectroscopic techniques. XPS analyzes materials down to its core electrons, giving it a great range of applications. XPS can identify all but two elements, H and He. XPS can also provide excellent quantitative analysis by use of established mathematical models. XPS can detect the difference in chemical states between samples and is able to differentiate the oxidation states of molecules.¹⁸ Not all techniques are perfect, and XPS has its fair share of disadvantages as well. XPS has a relatively large size limit of 10 μm . XPS must be done in ultra-high vacuum, meaning sample introduction time is generally longer than other techniques. XPS spectra also takes a long time to produce, meaning there will likely be long downtimes between running a sample and getting data.¹⁸

Given all the background information presented in this chapter, we can now move onto the experimental section with a better view of the importance of producing niobium oxide thin films for use as an ETM.

1. Experimental

3.1 Materials and Chemicals

All chemicals were not modified from their received state. The main chemical used was (t-Butylimido)tris(diethylamino)niobium(V) (98% TBTDEN, 5 g). The niobium compound was used as the precursor for the oxide deposition. A piranha solution of 33% hydrogen peroxide (H_2O_2 , 35% w/w aq. solution, Alfa Aesar) and 66% sulfuric acid (H_2SO_4 , technical Grade, Fisher Chemical) was used to clean wafers before being used for ALD. Isopropyl alcohol (IPA, 99.6%, Acros Organics) was used to clean grease off joints before ALD runs. Ultra-high purity (UHP) water obtained through a Mili-Q filtration system, which provided water at $18\text{M}\Omega$ cm resistivity (Millipore). Such water was used for cleaning and rinsing of joints and wafers. High temperature vacuum grease was used to grease all joints before ALD runs. UHP nitrogen gas (N_2 , Airgas) was used as the carrier gas. Degenerately doped n^+ -Silicon (n^+ -Si(111), Addison Engineering) was used as the substrate in all runs.

3.2 Wafer Preparation

I prepared n^+ - Si (111) wafers for ALD deposition using a piranha solution. First, I cut silicon wafers into a small, triangular shape using a scribe. I then transferred the wafers into small glass test tubes. I prepared the piranha solution by first placing 20 ml of sulfuric acid into a beaker. Then, I slowly placed 10 ml of hydrogen peroxide into the beaker. I mixed the solution and placed 1 to 2 milliliters into the test tubes. Once each wafer was sufficiently submerged in the piranha solution, I distributed the remaining solution among the tubes. I let the wafers sit in the solution for approximately 20 minutes. After 20 minutes, I flushed the piranha solution using distilled water. I flushed the wafers 5-6 times to ensure no piranha solution was left on the wafer. Once the wafers were flushed, they were transferred to a large centrifuge tube and stored in UHP water until use.

3.3 Atomic Layer Deposition

In the lab, an ALD device was fabricated in the lab fume hood. A schematic of such an ALD can be seen in Fig. 3.1.

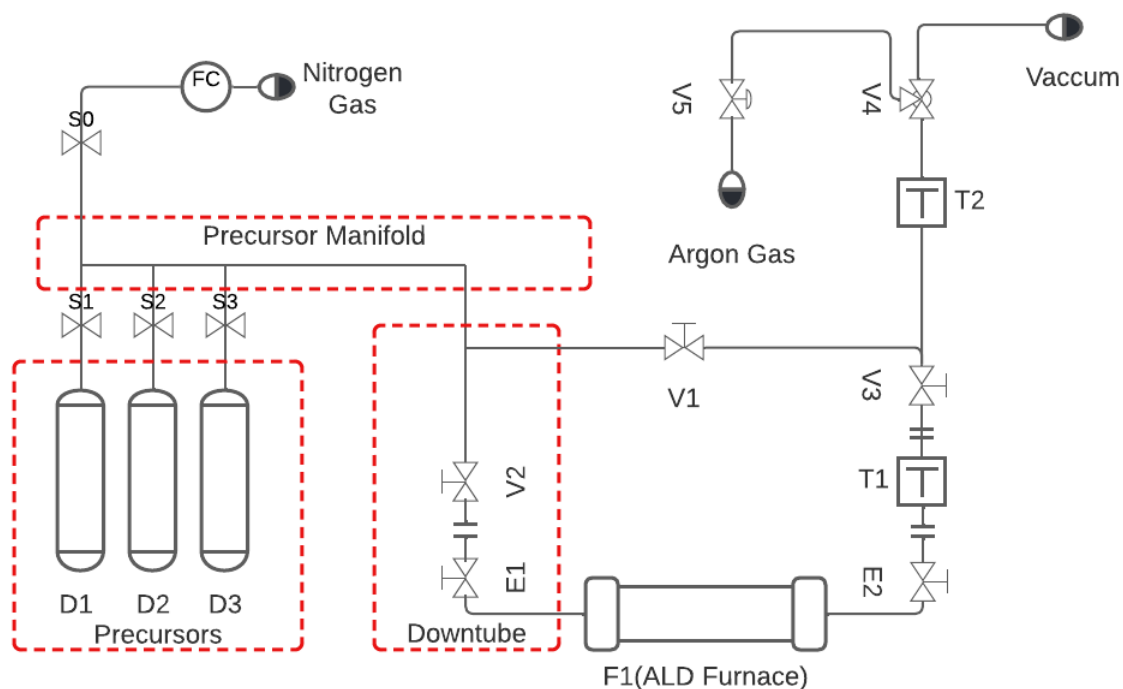


Figure 3-1: Process flow diagram of the Atomic Layer Deposition (ALD) instrument.

The 3 precursors are placed in custom made chambers, D1, D2, and D3. The chambers were built using ¼” male VCR fittings, ¼” male NPT connectors, SS-4-VCR-1-4 Swagelok valves, a 3” length of stainless-steel NPT pipe, a McMaster 4464K356 threaded pipe fitting, and a McMaster 4464K512 female NPT cap. Teflon tape was used at NPT fittings, and Hysol 1C epoxy was used at NPT-to-NPT connections to ensure a good seal. Precursor D1 contains water, D2 contains Tetrakis(ethylmethylamino)titanium(IV), and D3 contains (t-Butylimido)tris(diethylamino)niobium(V). The vessels are heated to the appropriate temperature to ensure the precursor inside is partially vapor. Each precursor vessel is connected to a solenoid that is controlled using the ALD’s main controller. The solenoids are MAC 34C-ABA-GDAV-1KT solenoids. The solenoids control Swagelok 6LVV-DPFR4-P-C 2-way valves that are connected to the precursor vessels. When pulsed by the computer, the solenoids open to the manifold, which is made from VCR fittings. The vapors are pushed down the downtube by

nitrogen gas controlled by an Aera FC-770AC analog Mass Flow Controller (MFC). V2 is a SS-4H Swagelok valve that allows for the ALD manifold and the ALD furnace to be cut off. Such a feature is needed when the ALD furnace is being loaded and open to vacuum. E1 and E2 are in-house elbow joints made by connecting a 24/40 TS male glass joint and a ¼" valve using glass blowing. F1 is a female-female 24/40 TS glass straight. The 3 precursors, manifold, downtube, and F1 are all heated using BriskHeat Heavy Insulated Heating Tapes (BIH0510020L and BIH051040L) and controlled by Dwyer Instruments Love 32B temperature controllers. Temperature was monitored by Nextel ceramic braid insulation K-type thermocouples from Omega Engineering. F1 was heated using two semicircular CRCF-series ceramic heaters by Omega Engineering. T1 and T2 are glass traps. V3 is another SS-4H Swagelok valve and is used to cut off the vacuum line to trap T1 when the trap is open to air. A more detailed description of the ALD setup can be found in Jocelyn Mendes' MQP thesis, §4.1-4.6.³⁰

3.4 Synthesis of Niobium Oxide Thin Film on n⁺-Si

An Atomic-Layer-Deposition system produced niobium oxide thin films on degenerately doped n⁺-Si (111) in a Grimmgroup lab fume hood. All abbreviations refer to Fig. 3.1. The following procedure was the general course of action for each run. First, I cleaned glass joints E1, E2, and F1 with IPA and laboratory wipes to remove any residual grease. I then removed the stopcock from E2 to clean it further. I greased the stop cock and the joint and reinserted the stopcock into E2, creating a good seal. After prepping E2, I prepared the wafer for a run. I removed a wafer from its storage in water and blew it with argon gas to remove any residual dust particles. I placed the wafer into F1 as close to the center as possible. I also ensured that the temperature probe was placed slightly in front of the wafer placement. I greased the open end of F1 and elbow E2 and placed them together to form an airtight seal. I turned the joint 4-5 times to ensure an airtight seal. A good seal was indicated by the grease forming a clear film in the joint. Once the joint was properly sealed, I pulled a vacuum on the system. To do this, I closed the stopcock on E1, opened V2, and closed the stopcock on E2. Then, I opened the stopcock on E1 slowly. Opening the valve too fast might have caused turbulence in the chamber, which could have caused the wafer to become displaced. After the E1 stopcock was fully opened, the pump pulled a vacuum on F1. Once a pressure of 30-50 mtorr was reached, it was safe to move on to the next step. To finish the setup, I greased the end of elbow E2 and connected it to trap T1 using

a silicon tube. I cut the tube to an appropriate length and secured the two ends using copper wire. I pulled a vacuum on the rest of the line by opening the valve on E2. Once the pressure reached a level of 30-50 mtorr again, I opened V3 and closed V1 to reach the running position. I placed liquid nitrogen baths under each of the traps. I covered both the traps with aluminum foil and fiber quartz to ensure minimum heat transfer to the environment. Finally, I closed the tube furnace that enclosed F1 to ensure minimum heat loss. A more detailed procedure can be found in §Appendix E.

The program has 3 presets of temperatures to set the ALD to. The presets were as follows:

Table 3-1: ALD Temperatures at 3 states; Standby, Pregame, and Running

Heated Area	Standby Temperatures (°C)	Pregame Temperatures (°C)	Running Temperatures (°C)
Manifold	140	140	140
D1 Precursor	50	50	50
D2 Precursor	115	115	115
D3 Precursor	100	100	100
Down Tube	160	160	160
ALD Furnace	0	150	150

I generally set the ALD running procedure as follows:

1. Set ALD furnace to specified “Running Temperatures” as defined in table X.
2. Wait X number of minutes. Wait time was generally set to 15-30 minutes, to allow for the ALD furnace to reach the specified temperature.
3. Set argon flow to 5 sccm. Such a value is changeable, however for all runs during these experiments, it was kept at 5.
4. Wait X number of minutes. The wait time was generally set to 15-30 minutes as well, to allow the system to settle.

5. Cycle X times, with each cycle being:
 - a. Pulse D1 (Water precursor), then wait 55 s
 - b. Pulse D3 (Niobium Precursor), then wait 55 s

Each pulse is defined as a sequence of micro pulses, which were as follows:

1. D1 pulse
 - a. 2 micro pulses at 20 milliseconds each, with a 980 ms wait
2. D3 pulse
 - a. 3 micro pulses at 50 milliseconds each, with a 500 ms wait.

Each micro pulse sends a signal to the solenoids S1, S2, or S3 to open for the given number of milliseconds.

6. Finish with a pulse of D1, then wait 5 seconds.
7. Set ALD to standby temperature as defined in table 3.1.
8. Set argon flow to 0 sccm.

After the run was completed, I ran 5 cycles of water precursor to ensure all niobium precursor was reacted. After a run, I pressurized the chamber to remove the sample. First, I cut off the ALD from the vacuum line. Next, I introduced argon gas to the system using V4 and V5. After 15-20 seconds of argon gas flow, I stopped the flow and removed E2 to gain access to the sample. I removed the sample using tweezers and placed it in a small centrifuge tube to be held until characterization.

3.5 XPS

To prepare the sample for XPS characterization I placed the sample on a sample puck. I used clean room gloved when using all mounting tools. First, I placed a holding tag on the sample puck. Next, I placed the wafer sample under the tag. I tightened the tag to ensure the sample didn't move when I introduced it into the XPS. Next, I placed the sample into the XPS load dock. The load dock was then pressured down to 1×10^{-7} torr. Once the load dock was pressurized, I introduced the sample to the XPS chamber, and characterization was started.

A PHI 5600 XPS system with a third-party data acquisition system (RBD Instruments, Bend Oregon) acquired all X-ray photoelectron (XP) spectra. Analysis chamber base pressures were around 1×10^{-9} torr. A hemispherical energy analyzer collected the X-ray photoelectrons. A monochromated Al K α source produced X-rays at a 90° angle with respect the takeoff angle for the energy analyzer. For the experiments, XPS data collection utilized a level sample puck that yields 45° angles both for the incoming monochromated X-radiation and for the photoelectron take-off angle with respect to the sample normal angle.³¹

In all experiments, survey spectra utilized a 117-eV pass energy, a 0.50 eV step size, and a 50 ms dwell time. All high-resolution XP spectra employed a 23.50 eV pass energy, 0.025 eV step size, and a 50 ms dwell time per step. X-ray photoelectron acquisitions included wide-energy survey scans as well as high-resolution scans of the Nb 3d, Si 2p, O 1s and C 1s regions for all samples. Once spectra were acquired, peak fitting was done using CasaXPS. I did peak fitting on the Nb 3d, O 1s, C 1s, and Si 2p peaks. I used Casa's wide quantification feature to fit the peaks and obtain areas. I created a new region and set the BG type to W Tougaard. I adjusted the region until the baseline covered most of the main peaks. §Appendix A contains all values used for peak fitting.

3.6 Overlayer Model Interpretation of Oxide Thickness

I employed a substrate overlay model to interpret X-ray photoelectron peak areas for the thickness of niobium oxide due to ALD deposition. The simplest overlayer model can be described as a substrate A, with a layer of material B layered over it, as illustrated in Fig. 3.2.



Figure 3-2: The Simplest Substrate-Overlayer Model

The model utilizes data gained from XPS to characterize the thickness of each layer. The model starts with an equation for a monolayer.

$$I_A = I_0 \sigma_A T(E_A) D(E_A) N_A \lambda_A \cos \theta \exp\left(\frac{-d_B}{\lambda_{A,B} \cos \theta}\right) \quad (3.1)$$

In eq 3.1, I_A is the intensity of element A, I_0 is the density of photons striking the surface per second, σ_A is the photoionization cross section from element A at energy $h\nu$. $T(E_A)$ is the ratio of electrons at energy E that enter the system versus the electrons that end up making it to the detector. $D(E_A)$ is the detector efficiency for electrons with energy E . N_A is the number density of atom A. The λ_A is the attenuation length of an electron from atom A traveling through pure material A. The $\lambda_{A,B}$ is the attenuation length of an electron ejected from substrate A traveling through overlayer B. d_B is the depth of layer B. Finally, θ is the emission angle of the electrons. The equation for the intensity of layer B can be described similarly to eq 3.1.

$$I_B = I_0 \sigma_B T(E_B) D(E_B) N_B \lambda_B \cos \theta \left(1 - \exp\left(\frac{-d}{\lambda_B \cos \theta}\right)\right) \quad (3.2)$$

A ratio between them can be expressed as eq 3.3.

$$\frac{I_B}{I_A} = \frac{I_0 \sigma_A T(E_A) D(E_A) N_A \lambda_A \cos \theta \exp\left(\frac{-d_B}{\lambda_{A,B} \cos \theta}\right)}{I_0 \sigma_B T(E_B) D(E_B) N_B \lambda_B \cos \theta \left(1 - \exp\left(\frac{-d}{\lambda_B \cos \theta}\right)\right)} \quad (3.3)$$

There are several terms that can be canceled out to make the equations easier to work with. First, the analyzer used is configured in fixed analyzer transmission mode. Such a mode means that all

electrons that make it to the detector arrive with similar energies. Therefore, the terms $T(E)$ and $D(E)$ can be canceled out. I_0 and the $\cos \theta$ terms outside of the exponent cancel out because the spectra are acquired at the same time, in the same machine, and in the same conditions.

Finally, the σ and λ terms outside the exponent can be combined into one term known as the sensitivity factor, SF. SF is tabulated for most elements for specific instrument configurations.

Taking all the simplifications into account, eq 3.3 can be reduced to eq 3.4.

$$\frac{I_B}{I_A} = \frac{N_B SF_B}{N_A SF_A} \frac{1 - \exp\left(\frac{-d_B}{\lambda_B \cos \theta}\right)}{\exp\left(\frac{-d_B}{\lambda_{A,B} \cos \theta}\right)} \quad (3.4)$$

Equation 3.4 is the simplest form of an overlayer model, but for the circumstances in this paper, a more complicated scenario must be considered.

For the research in this paper with niobium pentoxide thin films, the substrate-overlayer model can be expressed as in Fig. 3.3.

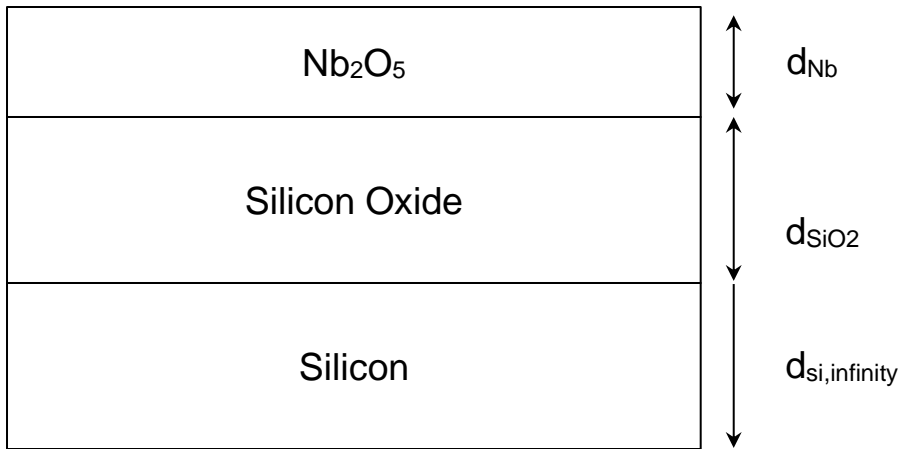


Figure 3-3: Niobium Pentoxide over-layer model

The system can be modeled by an equation like eq 3.4 but modified to fit the 3rd layer. The relationship between the niobium pentoxide layer and the silicon substrate can be expressed by eq 3.5.

$$\frac{I_{Nb}}{I_{Si}} = \frac{N_{Nb} SF_{Nb}}{N_{Si} SF_{Si}} \frac{1 - \exp\left(\frac{-d_{Nb}}{\lambda_{Nb} \cos \theta}\right)}{\exp\left(\frac{-d_{SiO_2}}{\lambda_{Si, SiO_2} \cos \theta}\right) \left(\exp\left(\frac{-d_{Nb}}{\lambda_{Si, Nb} \cos \theta}\right)\right)} \quad (3.5)$$

In eq 3.5, N_{Nb} , N_{Si} , the sensitivity factors, and the attenuation lengths are found in the literature or through experimentally obtained equations. The attenuation length can be found through experimentally obtained models with eq 3.6.

$$\lambda_x = 3.16 \times 10^{11} nm \left(\frac{\langle A \rangle}{\rho N}\right)^{0.5} \left[\frac{E}{\langle Z \rangle^{0.45} (3 + \ln(\frac{E}{27}))} + 4 \right] \quad (3.6)$$

In eq 3.6, $\langle A \rangle$ is the average molar mass in grams per mole, ρ is the density of the pure element in kilograms per meter cubed, N is Avogadro's number in mol^{-1} , E is the photoelectron kinetic energy, and $\langle Z \rangle$ is the average atomic number of the element or compound. E can be found using machine parameters and the binding energy of the element, as expressed in eq 3.7.

$$E = KE - BE - \Phi_D \quad (3.7)$$

KE is the kinetic energy of the XPS machine and is dependent on which anode is used. BE is the binding energy of the element and can be generally found in literature. Finally, Φ_D is the work function of the XPS machine. The depth of the oxide layer, d_{SiO_2} , can be found experimentally using eq. 3.8. The equation came from previous experimentation from the PHI 5600 XPS in the laboratory, therefore the numbers in the equation are specific to that machine.

$$d_{\text{SiO}_2} = 2.464 \text{ nm} \ln\left(1.41 \frac{I_{\text{Ox}}}{I_{\text{Si}}} + 1\right) \quad (3.8)$$

The intensity of the oxide and the silicon, I_{Ox} and I_{Si} , can be found experimentally using XPS. Peak intensities can be found using analytical software such as Casa. The number densities can be found using eq. 3.9.

$$N_x = \frac{\text{Number of X Atoms in Unit Cell}}{\text{Volume of Unit Cell}} \quad (3.9)$$

The number of atoms in each unit cell can be found in literature or through a crystal modeling software such as VESTA. The silicon unit cell used is illustrated in Fig. 3.4.

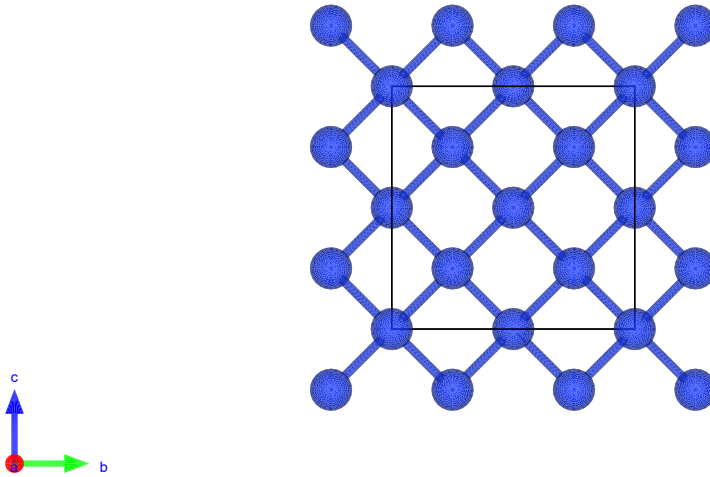


Figure 3-4: Silicon Cubic Unit Cell Modeled in VESTA

The silicon unit cell has 4 atoms on the edge, making for $\frac{1}{4} \times 4 = 1$ atoms. 4 atoms are on the face which equals $\frac{1}{2} \times 4 = 2$ atoms. 5 atoms are contained completely in the unit cell. This gives a unit cell containing 8 atoms. Silicon is a cubic unit cell, meaning all side are equal. a, b, and c are equal to 0.543 nm, making for a volume V_{si} equal to 1.629 nm^3 . For use in equation 3.5, the number density of silicon, N_{si} , is needed. N_{si} can be found using equation 3.9. N_{si} is equal to 49.943 nm^{-3} .³²

The niobium pentoxide unit cell is illustrated by Fig. 3.5.

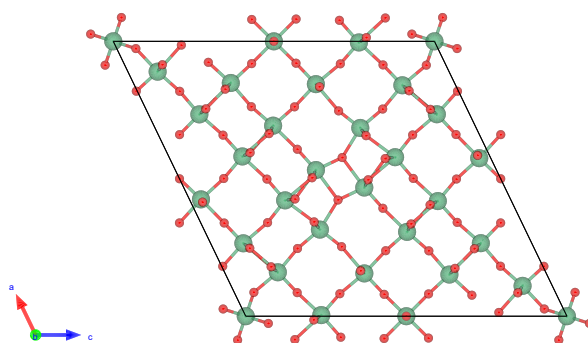


Figure 3-5: Niobium Pentoxide Unit Cell Modeled in VESTA

Niobium pentoxides unit cell contains 28 atoms. The parameters of the unit cell were found to be $a_{\text{Nb}_2\text{O}_5} = 0.3872 \text{ nm}$, $b_{\text{Nb}_2\text{O}_5} = 1.9789 \text{ nm}$, and $c_{\text{Nb}_2\text{O}_5} = 2.0814 \text{ nm}$.³³ The lengths give a unit cell volume of 1.456 nm^3 . Using eq 3.9, $N_{\text{Nb}_2\text{O}_5}$ is equal to 6.90262 nm^{-3} .

In eq 3.5, I took several numbers from literature. The sensitivity factors of niobium and silicon I used are 2.517 and 0.283 respectively.²⁸ I found in literature the attenuation length of Si 2p electrons through silicon oxide, $\lambda_{\text{Si,SiO}_2}$, to be 3.485 nm.⁷ I found the attenuation length of Nb 3d electrons through Nb_2O_5 , λ_{Nb} , both in literature and calculated using eq 3.6. I found the literature value to be 5.8 nm.³⁴ For use in eq 3.6, I found $\langle A \rangle$ to be 37.97 g mol^{-1} , $\rho_{\text{Nb}_2\text{O}_5}$ to be 4550 kg m^{-3} , N to be $6.03 \cdot 10^{23}$, and $\langle Z \rangle$ to be 17.43. I found E using eq 3.7. I found KE to be 1486.6. Such a value is the kinetic energy of a monochromated Al K α X-Ray source. I found the binding energy of niobium to be 202.4 eV.²⁸ Finally, I found the work function (Φ_D) of the XPS instrument to be equal to 3 eV. Plugging into equation 3.7, I found E to be 1,281 eV. Plugging everything into eq 3.6, I got a value for λ_{Nb} of 2.07 nm. I calculated the attenuation length of Si 2p electrons traveling through Nb_2O_5 , $\lambda_{\text{Nb,Si}}$, using eq 3.6 as well. I found $\langle A \rangle$ to be 92.9 g mol^{-1} , $\rho_{\text{Nb}_2\text{O}_5}$ to be 4550 kg m^{-3} , N to be $6.03 \cdot 10^{23}$, and $\langle Z \rangle$ to be 14. I found E similarly to λ_{Nb} , but with a binding energy of 99 eV. I found E to be 1,387 eV. Figure 3.6 shows the result of solving equation 3.5.

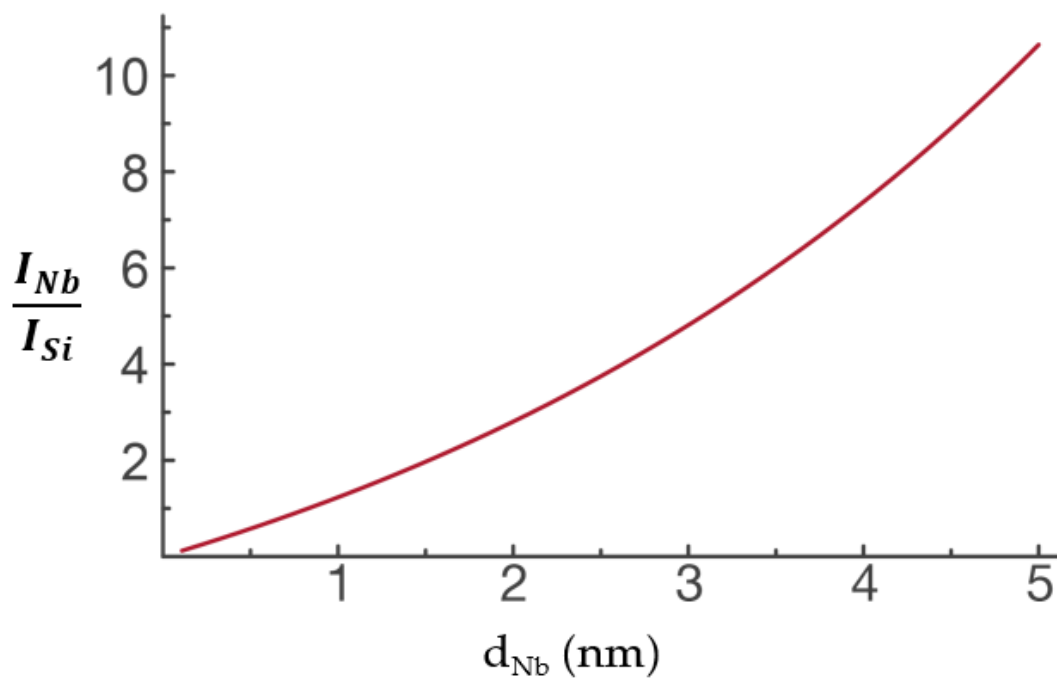


Figure 3-6: Theoretical Graph of the Silicon/Niobium Intensity Ratio vs the Thickness of Niobium Pentoxide.

All equations used in this chapter were adapted from Alex Carl's thesis paper.⁷

Using Mathematica's solve function, the silicon oxide thickness of 2.27 nm can be used to get a niobium pentoxide thickness of 1.22 nm.

4.2 Overlay Model Results

Samples AR-4,6,7,9,10,11, and 13 were run with a 15-minute initial wait and a 15-minute secondary wait, giving a total initial wait time of 30 minutes. Each sample was run for 20 cycles and D1 and D3 had a 55 second wait time in between pluses. The furnace was set to 150 °C. These samples are labeled as set 1.

Table 4-1: Data for Set 1 Involving 20 cycles at 150 °C

Sample	Nb/Si Ratio	Ox/Si ratio	Oxide Thickness (nm)	Nb ₂ O ₅ layer thickness (nm)
AR4	0.481	0.659	1.60	0.999
AR6	0.242	0.814	1.88	1.10
AR7	0.411	0.994	2.16	1.19
AR9	0	0.523	1.36	n/a
AR10	0	1.12	2.34	n/a
AR11	0	0.925	2.06	n/a
AR13	0	0.673	1.64	n/a

4 of the 7 samples show niobium growth. The standard deviation of the Nb/Si ratio among the 3 samples that have growth is 0.100. For all 7 samples, the standard deviation of the O/Si ratio is 0.195 and for oxide thickness, 0.322. Finally, for the 3 samples that show niobium growth, the standard deviation of calculated thickness is 0.0780.

Samples AR-16, 17,18,19, 20, 22, and 23 were run with a 30-minute initial wait and a 30-minute secondary wait. This gives a total wait time of 1 hour. Each sample was run for 20 cycles and D1 and D3 had a 55 second wait time in between pluses. The furnace was set to 150 °C. These samples are labeled as set 2.

Table 4-2: Data for Set 2 Involving 20 cycles and 150 °C

Sample	Nb/Si Ratio	Ox/Si ratio	Oxide Thickness (nm)	Nb ₂ O ₅ layer thickness (nm)
AR16	0.222	1.07	2.27	1.22
AR17	0.151	0.629	1.57	0.984
AR18	0	0.729	1.74	n/a
AR19	0	0.850	1.94	n/a
AR20	0	0.767	1.81	n/a
AR22	0.162	0.743	1.77	1.06
AR23	0.355	0.442	1.19	0.821

4 of the 7 samples in set 2 showed niobium growth. The standard deviation of the Nb/Si ratios among samples that have niobium growth is 0.0811. For all samples, the standard deviation of the O/Si ratio is 0.178 and 0.306 for oxide thickness. For samples that have niobium growth, the standard deviation of the calculated thickness is 0.143.

Samples AR 31 and 32 were run with a 30-minute initial wait and a 30-minute secondary wait time, giving a total wait time of 1 hour. Each sample was run for 30 cycles and D1 and D3 had a 55 second wait time in between pluses. The furnace was run at 150 °C. These samples are labeled as set 3.

Table 4-3: Data for set 3 Involving 30 cycles and 150 °C

Sample	Nb/Si Ratio	Ox/Si ratio	Oxide Thickness (nm)	Nb ₂ O ₅ layer thickness (nm)
AR-31	0	1.25	2.51	n/a
AR-32	0	0.867	1.97	n/a

None of the samples in set 3 had niobium growth. The standard deviation of the O/Si ratio is 0.192. The standard deviation in the oxide thickness is 0.27.

AR25-30 are runs with more than one sample. Figure 4.2 illustrates the two different exposure patterns the 2-wafer runs were set in.

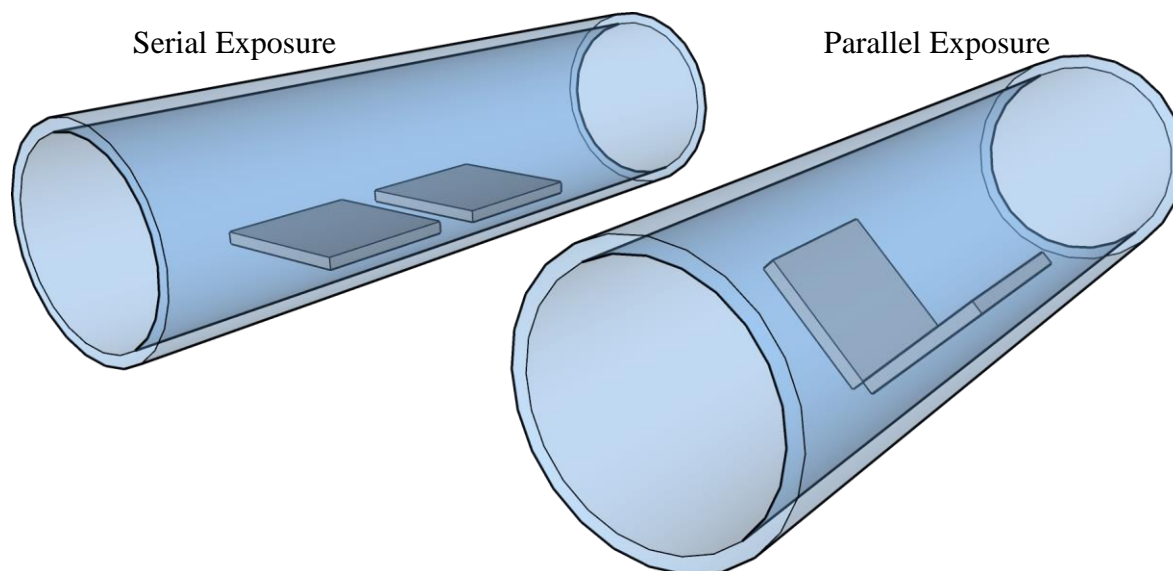


Figure 4-2: Serial and Parallel exposure set-up of AR25-30

AR25, AR26, AR29 and AR30 were run in serial exposure. AR27 and AR28 were run in parallel exposure. All samples were run with a 30-minute initial wait and a 30-minute secondary wait. This gives a total wait time of 1 hour. Each sample was run for 20 cycles and D1 and D3 had a 55 second wait time in between pluses. The furnace was set to 150 °C. These samples are labeled as set 4

Table 4-4: Data from Serial Exposure Runs in Set 4 Involving 20 cycles and 150 °C

Sample	Nb/Si Ratio	Ox/Si ratio	Oxide Thickness (nm)	Nb ₂ O ₅ layer thickness (nm)
AR25	0.203	0.952	2.10	0.559
AR26	0.264	1.87	3.18	0.450
AR29	0	0.918	2.04	n/a
AR30	0	0.975	2.13	n/a

Table 4-5: Data from Parallel Exposure Runs in Set 4 Involving 20 cycles and 150 °C

Sample	Nb/Si Ratio	Ox/Si ratio	Oxide Thickness (nm)	Nb ₂ O ₅ layer thickness (nm)
AR27	0.300	0.831	1.91	1.11
AR28	0	1.52	2.82	n/a

For samples in series, only one set of runs showed growth. The other 2 sample run, which had the same parameters as AR25 and 26, does not have growth. For samples that have niobium growth, the standard deviation in the Nb/Si ratio is 0.0305. The standard deviation of the layer thickness is 0.0545. For all samples, the standard deviation of the O/Si ratio is 0.399 and for oxide thickness is 0.473. For samples in tandem, only one of the samples has growth. The standard deviation of the O/Si ratio is 0.345 and for oxide thickness is 0.455.

AR 5, 21, and 24 were ran with slightly different parameters and do not fit into any set. AR-5 was run with the same parameters as set 1, but with 10 cycles. AR 21 was run with the same parameters as set 2, but with a furnace temperature of 175 °C. Finally, AR-24 is like set 2 as well, but with a wait time after D3 pulse of 75 seconds.

Table 4-6: Data for other samples

Sample	Nb/Si Ratio	Ox/Si ratio	Oxide Thickness (nm)	Nb ₂ O ₅ layer thickness (nm)
AR5	0.231	0.622	1.55	0.979
AR21	0	0.961	2.11	n/a
AR24	0	2.13	3.42	n/a

4.3 Pressure Results

The pressure for 3 runs is shown in Fig. 4.3 and 4.4. Pressures are expressed in millitorr.

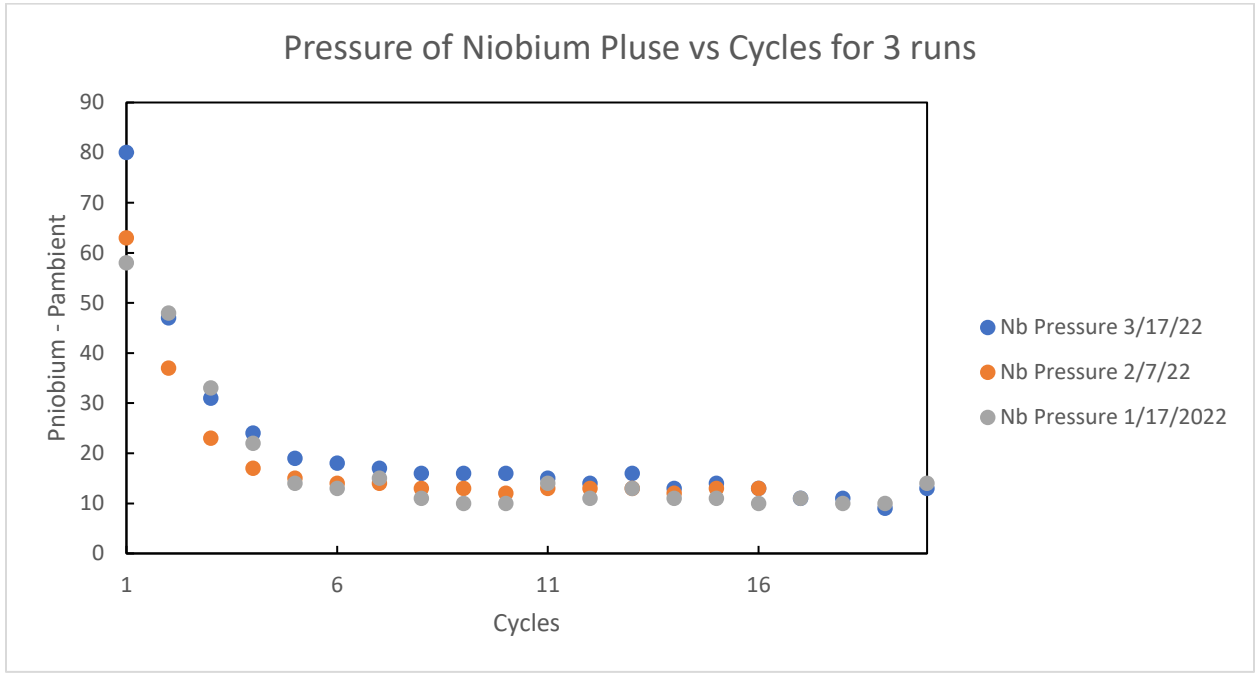


Figure 4-3: Pressure of Niobium vs Idle Running Pressure for 3 Separate Runs

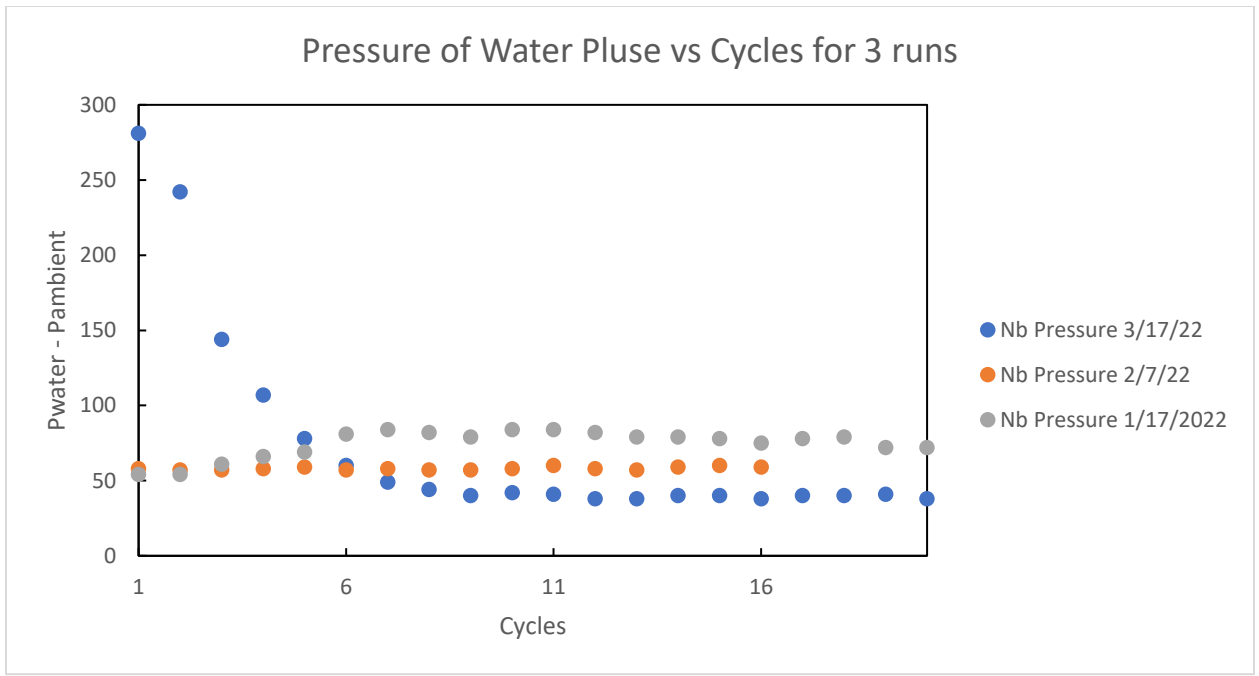


Figure 4-4: Pressure of Water vs Idle Running Pressure for 3 Separate Runs

For both Fig. 4.3 and 4.4, each color represents a different run. The run on 1/17/2022 is AR-4, on 2/7/22 is AR-16, and on 3/17/22 is AR-23. All 3 runs showed niobium deposition. Table 4.7 shows the resulting growth from the 3 runs shown in Fig. 4.3 and 4.4.

Table 4-7: Data from AR-4, AR-16, and AR-23

Sample	Nb/Si Ratio	Ox/Si ratio	Oxide Thickness (nm)	Nb ₂ O ₅ layer thickness (nm)
AR4	0.481	0.659	1.60	0.999
AR16	0.222	1.07	2.27	1.22
AR23	0.355	0.442	1.19	0.821

Since the runs are not all under the same conditions, it is not valid to discuss standard deviations among the samples.

4.4 Contamination Analysis

Carbon levels were looked at to assess contamination issues. Figure 4.5 shows the ratio of C to Si and Nb to Si for each sample, regardless of running parameters.

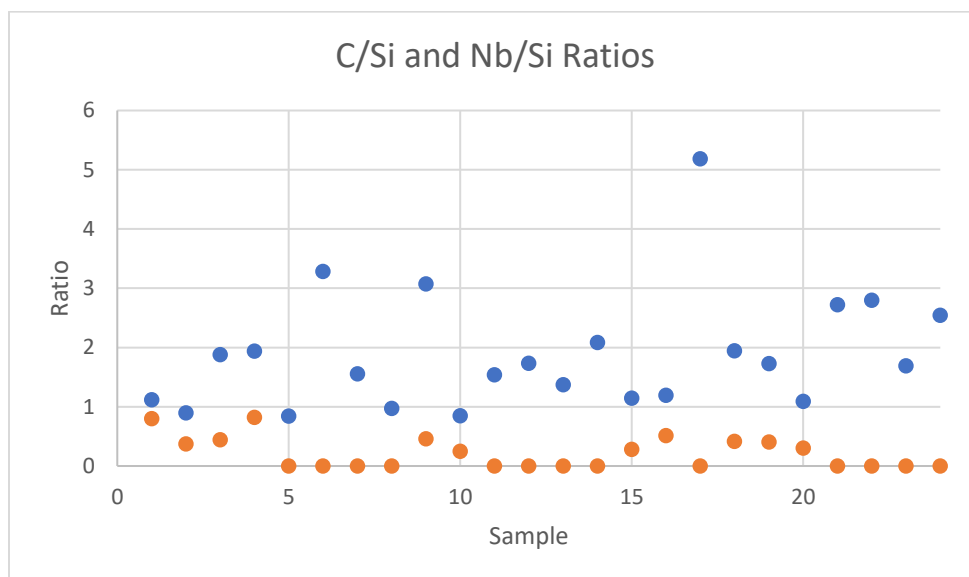


Figure 4-5: Carbon and Niobium Ratios for All Samples

In Fig. 4.5, the blue dots represent the C to Si ratio. A higher ratio means more carbon on the surface, and therefore more contamination. The orange dots represent the Nb to Si ratio. Any non-zero number here means that niobium growth was obtained.

5. Discussion

While deposition was achieved, the results were inconsistent. Throughout all runs, only 9 showed deposition of niobium at a detectable level, despite nearly identical running conditions among sets. When looking at reasons for inconsistency, there are many factors that can be considered. The first factor that was explored was looking at the wait times before deposition, which can be seen in the difference between set 1 and set 2. There are two wait times that can be changed. The time for the furnace to reach temperature and stabilize, and the time for when flow is activated. The initial wait time was set to 15 minutes. Although this was enough time to get the furnace to the desired temperature, it is possible that such a time is not long enough to let all the system stabilize to the right temperature. When elbow E1 is replaced, it might take more time for it to reach temperature again. Also, the thermocouple is placed in the middle of the tube furnace, but all areas might not reach the desired temperature at the same time. The entrance and exit to the furnace might take especially long to reach desired temperatures. Because of such reasons, the initial wait time was set to 30 minutes to give the system more time to stabilize. The wait time after flow was activated was also set to 30 to let the system equilibrate longer. Although more consistent growth was achieved after the change, growth was still inconsistent overall. As seen in table 4.2, AR16 and 17 showed growth directly after the wait time change. However, after AR17, growth stops again until AR21. Therefore, we cannot verify that changing the wait times directly lead to more consistent growth.

Another parameter that may affect consistent growth is the pressure of the experiments. If the niobium is not reaching the deposition chamber, then there will be no niobium deposited onto the surface. Also, if there is not enough vapor pressure at the top of either precursor vessel, then deposition will not happen. When analyzing the pressure, we can see that the pressure vs counts graph, Fig. 4.3, during 3 different experiments roughly a month apart stays similar. Such a result is a good indication that pressure is not a problem in terms of deposition. These data are also a good indicator that the niobium precursor has not been depleted, which was an unlikely but possible issue. One thing we can note about pressure is that it is not identical for all 3 experiments, and it decreases as counts go on. In all 3 experiments, the difference in the ambient pressure and the pressure when niobium was pulsed reached steady state at around the same range of 10-15 mtorr. The first 5 cycles show some variability in pressure difference between the experiments. Such variability could be a reason why niobium thickness is not closer among

samples. When looking at the water pluses, the variability is greater. The experiment on 3/17/22 shows a similar pattern to the niobium pressure, while the other ones have a mostly flat line. The steady state of the runs is also further apart compared to the niobium pluses. Such variability also contributes to the difference in niobium thickness among 20 cycle experiments. If it is desired to change the pressure in future experiments, then a higher ambient argon flow or higher precursor temperatures would be the best ways to achieve this.

ALD deposition can be hindered by cold spots present in the system. If there is a cold spot present, then the niobium will deposit prematurely. In our case, the area around elbow E1 has potential for many cold spots if not insulated properly. The area around E1 is heavily insulated with fiber-quartz and tin foil to contain as much heat as possible. There is no way to quantify the heat loss in the lab with the current equipment, so each experiment was insulated as close to the last as possible. Even with similar insulation throughout each experiment, deposition was still inconsistent. Such a result indicates that insulation is not the issue in terms of deposition. Heat loss can be explored in future experiments with the use of thermocouples placed more closely to elbow E1. The thermocouples will help to ensure temperature is consistent and not dropping at any point. The reaction temperature also has a large effect on deposition. If the temperature is too low, the reaction might not occur. If the temperature is too high, products might decompose. For most experiments, 150 °C was used as the furnace temperature. 150 °C was the agreed upon number in several papers on growing niobium with ALD.³⁵ However, such papers had commercial ALDs. The ALD we are working with likely has different parameters, as it was built in house. Although 150 °C showed deposition, it was not consistent. Experimenting with more temperatures might lead to more consistent growth.

Deposition can be affected by the contamination on the silicon substrate. If there is a lot of grease and other contaminants on the surface, then there will be less available binding sites for the niobium. Contamination could also come from the wafer cleaning process itself. If the piranha solution is not completely cleaned off before removing the wafers with tweezers, it is possible that the piranha will dissolve the tweezers onto the wafer. There is no good way to tell if the piranha solution is off the wafer. The best way to prevent tweezer contamination is to wash the wafers in water as sufficiently as possible. In Fig. 4.5, a comparison of carbon levels to niobium levels is illustrated. It is hard to see a relation between the carbon levels and niobium growth. Samples such as 6 and 17 show high levels of carbon and no niobium growth. However,

sample 9, which showed niobium growth, has a similar ratio of C/Si as sample 6, which did not have niobium growth. Because of discrepancies like such, it is difficult to be able to point to contamination being the major issue of inconsistent niobium growth. It is possible the contamination is non-organic and therefor would not show up in carbon levels.

6. Future directions

Future work on this project can involve many things. First, looking further into contamination issues is key. To do this, making sure the wafer fabrication process is done as cleanly as possible is key. Looking at more spots on the sample will also help to see if the contamination is everywhere. Since XPS is spot specific, you are only getting information on the very specific area you are analyzing. If 3-5 spots were taken per wafer, more data would be gathered. This will take more time to run, but it will be beneficial to gain more data points. If it is determined that organic based contamination is not present, then it may be beneficial to look at non-organic contamination sources. If it is ruled out that wafer contamination is not an issue, it would be beneficial to look further into the ALD setup itself. Issues with cold spots or grease contamination can also be looked at. If there are blockages in the system, then the growth will be impeded. E1 has potential to have a lot of contamination. Because E1 is not typically replaced after every run, grease build up in the stopcock joint is more likely. The silicon tube connecting E1 to the downtube also has potential to come lose or be angled in an odd way. It would be beneficial to replace and clean this tube every run and see if that makes growth more consistent. Such a procedural change will add more time to the overall procedure, but if it leads to consistent niobium growth, then it is a necessary addition.

More experiments on temperature would also be beneficial. Looking at temperatures from 130 °C – 175 °C and analyzing growth at each would help find a more ideal deposition temperature. Such an experiment would include testing temperatures from 130 °C -175 °C in 5-degree increments. Running 3-5 samples at each temperature will ensure good data.

Once consistency issues are solved, looking at more cycles runs is the next step. This would involve doing 30,50, and 100 cycles at ideal parameters, with 3-5 wafers per cycle. Next, the cycle count vs niobium thickness gained from my Mathematica notebook can be plotted. This plot will be able to give the ideal conditions to yield 2 nm film thickness. The 2 nm thickness is the hypothetical required thickness for passivation of the silicon surface.

R.S. F	1	1	1	1	1	1	1	1
Line Shape	GL (30)	GL (30)						
Area Constr.	0.0, 10,000,000	A*0.5	0.0, 10,000,000	C*0.5	0.0, 10,000,000	E*0.5	0.0, 10,000,000	G*0.5
fwhm Constr.	0.2702, ??	A*1	A*1	A*1	0.2,5	E*1	E*1	E*1
Position Constr.	108,95	A+0.6 1	108,95	C+0.6 1	108,95	E+0.6 1	108.95	G+0.6 1

Appendix B: Mathematica Notebook

```

In[1]=  $\theta = \frac{\pi}{4}$ ; (* Takeoff angle in radians *)

In[2]= SiUnitCellLength = 0.543090; (* Units are nanometers *)

In[3]=  $\rho_{Si} = \frac{8}{\text{SiUnitCellLength}^3}$  (* Units are atoms nm-3 *)

Out[3]= 49.943

In[4]= (* Niobium unit cells lengths in nanometers*)
aNb = 0.3872;
bNb = 1.9789;
cNb = 2.0814;
NbUnitCellVolume = aNb * bNb * cNb;

In[8]=  $\rho_{Nb} = \frac{28}{\text{NbUnitCellVolume}^3}$  (* Units are atoms nm-3 *)

Out[8]= 6.90262

In[9]= (* Sensitivity factors for Phi 5600 instrument with OmniFocus III analyzer and mono illumination *)
SFSi = 0.283;
SFNb = 2.517;
(* Attenuation lengths in nm*)
 $\lambda_{Si}$ self = 2; (* Attenuation length of Si2p through bulk silicon *)
 $\lambda_{SiOx}$ self = 3.485; (* Attenuation length of Si2p through silicon oxide *)
 $\lambda_{Nb}$ lit = 5.8; (* Attenuation length of Nb3d through Nb205 itself from https://accelconf.web.cern.ch/SRF97/papers/srf97d18.pdf *)
NbAvgAtomicNumber = (41 * (2 / 7)) + (8 * (5 / 7))
NbAvgMolarMass = (92.90637 * (2 / 7)) + (16.00 * (5 / 7))

Out[14]=  $\frac{122}{7}$ 

Out[15]= 37.9732

In[16]= Nb205density = 4550; (* kg m-3*)


$$\lambda_{Nb}calc = 0.316 * 10^{12} \left( \frac{\text{NbAvgMolarMass}}{\text{Nb205density} * 6.02 * 10^{23}} \right)^{1/2} \left( \frac{1486 - 202}{\text{NbAvgAtomicNumber}^{0.45} * (3 + \text{Log}[\frac{1486 - 202}{27}])} + 4 \right)$$


Out[17]= 2.07269

In[18]=  $\lambda_{Nb}$ self =  $\lambda_{Nb}$ lit;

In[19]=  $\lambda_{Si}$ Nbcalc = .316 * 1012  $\left( \frac{92.9}{\text{Nb205density} * 6.02 * 10^{23}} \right)^{1/2} \left( \frac{1486 - 99}{14^{0.45} * (3 + \text{Log}[\frac{1486 - 99}{27}])} + 4 \right)$  (* Si 2p electrons going through Nb205 *)

Out[19]= 3.78017

In[20]=  $\lambda_{Si}$ Nbguess =  $\lambda_{Nb}$ lit

Out[20]= 5.8

In[21]=  $\lambda_{Si}$ Nb =  $\lambda_{Si}$ Nbguess

Out[21]= 5.8

In[48]= ExperimentalOxIntensityRatio = 1.866216 (* from 01 ar06 20 cycle run nb on n+Si wafer multi.vms*)

Out[48]= 1.86622

In[49]= OxideThickness[experimentalRatio_] := 2.464 * Log[(1.41 * (experimentalRatio)) + 1] (* experimental ratio obtained from XPS, Iox/Isi *)
OxideThickness[ExperimentalOxIntensityRatio]

Out[50]= 3.1776

In[25]=

In[26]= NiobiumIntensity[d_] :=  $\rho_{Nb} * \text{SFNb} * \left( 1 - \text{Exp}\left[\frac{-d}{\lambda_{Nb}self * \text{Cos}[\theta]}\right]\right)$ 

```

In[27]= `SiliconIntensity[d_, ER_] := $\rho_{\text{Si}} * S_{\text{FSi}} * \text{Exp}\left[\frac{-(\text{OxideThickness}[ER])}{\lambda_{\text{SiOxself}} * \text{Cos}[\theta]}\right] * \left(\text{Exp}\left[\frac{-(d)}{\lambda_{\text{SiNb}} * \text{Cos}[\theta]}\right]\right)$`

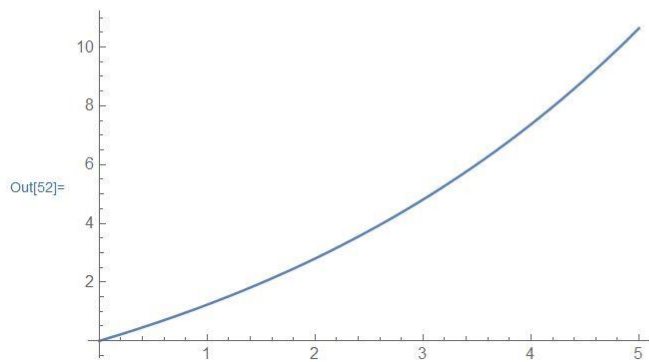
In[51]=

`Solve[NiobiumIntensity[d] / SiliconIntensity[d, ExperimentalOxIntensityRatio] == 1.866216, d]`

`Plot[NiobiumIntensity[x] / SiliconIntensity[x, ExperimentalOxIntensityRatio], {x, 0, 5}]`

`Solve`: Inverse functions are being used by Solve, so some solutions may not be found; use Reduce for complete solution information.

Out[51]= `{{d -> 1.43273}}`



Appendix C: Raw Peak Areas from Experiments

AR04			AR05			AR06			AR07			AR08			AR09			AR10		
Compound	Peak ID	Peak Area																		
Nb	A	1329.5	Nb	A	1004.1	Nb	A	684.6	Nb	A	505.5	Nb	A	N/a	Nb	A	N/a	Nb	A	N/a
Nb	B	886.3	Nb	B	669.4	Nb	B	456.4	Nb	B	337	Nb	B	N/a	Nb	B	N/a	Nb	B	N/a
Nb	Total	2215.8	Nb	Total	1673.5	Nb	Total	1141	Nb	Total	842.5	Nb	Total	0	Nb	Total	0	Nb	Total	0
Si	Si	900.5	Si	Si	2540.7	Si	Si	1568.1	Si	Si	608.6	Si	Si	N/a	Si	Si	672.6	Si	Si	1016.5
Si	Si	450.2	Si	Si	1270.4	Si	Si	784.1	Si	Si	304.3	Si	Si	N/a	Si	Si	336.3	Si	Si	508.2
Si	Si	954.7	Si	Si	436.8	Si	Si	151.2	Si	Si	75.7	Si	Si	N/a	Si	Si	0	Si	Si	0
Si	Si	472.8	Si	Si	218.4	Si	Si	75.6	Si	Si	37.9	Si	Si	N/a	Si	Si	0	Si	Si	0
Si	Si Total	2778.2	Si	Si Total	4466.3	Si	Si Total	2579	Si	Si Total	1026.5	Si	Si Total	0	Si	Si Total	1008.9	Si	Si Total	1524.7
Si	SiO	1220.6	Si	SiO	1852.1	Si	SiO	1289.4	Si	SiO	132.8	Si	SiO	N/a	Si	SiO	352	Si	SiO	1145.4
Si	SiO	610.3	Si	SiO	926.1	Si	SiO	809.1	Si	SiO	887.9	Si	SiO	N/a	Si	SiO	176	Si	SiO	572.7
Si	SiO total	1830.9	Si	SiO total	2778.2	Si	SiO total	2098.5	Si	SiO total	1020.7	Si	SiO total	0	Si	SiO total	528	Si	SiO total	1718.1
O	A	9377.6	O	A	16899.6	O	A	754.7	O	A	5719.4	O	A	N/a	O	A	6062.8	O	A	8889.5
O	B	1523.1	O	B	0	O	B	11241.8	O	B	564.6	O	B	N/a	O	B	241.5	O	B	1295.8
O	Total	10900.7	O	Total	16899.6	O	Total	11996.5	O	Total	6284	O	Total	0	O	Total	6304.3	O	Total	10185.3
C	A	2790.3	C	A	2839.8	C	A	4032.9	C	A	817.7	C	A	N/a	C	A	567.5	C	A	4600.2
C	B	0	C	B	583.5	C	B	623.8	C	B	1030.3	C	B	N/a	C	B	200.2	C	B	408.4
C	C	311.2	C	C	589.9	C	C	183.7	C	C	140.4	C	C	N/a	C	C	81.2	C	C	0
C	Total	3101.5	C	Total	4013.2	C	Total	4840.4	C	Total	1988.4	C	Total	0	C	Total	848.9	C	Total	5008.6
AR11			AR12			AR13			AR14			AR15			AR16			AR17		
Nb	A	N/a	Nb	A		Nb	A	N/a	Nb	A		Nb	A		Nb	A	499.4	Nb	A	512.1
Nb	B	N/a	Nb	B		Nb	B	N/a	Nb	B		Nb	B		Nb	B	332.9	Nb	B	341.4
Nb	Total	0	Nb	Total	832.3	Nb	Total	853.5												
Si	Si	1401.9	Si	Si		Si	Si	1989.4	Si	Si		Si	Si		Si	Si	1204.4	Si	Si	209.5
Si	Si	701	Si	Si		Si	Si	994.7	Si	Si		Si	Si		Si	Si	602.2	Si	Si	1475.7
Si	Si	171.7	Si	Si		Si	Si	254.5	Si	Si		Si	Si		Si	Si	0	Si	Si	737.8
Si	Si	85.9	Si	Si		Si	Si	127.3	Si	Si		Si	Si		Si	Si	0	Si	Si	1036.3
Si	Si Total	2360.5	Si	Si Total	0	Si	Si Total	3365.9	Si	Si Total	0	Si	Si Total	0	Si	Si Total	1806.6	Si	Si Total	3459.3
Si	SiO	1455.8	Si	SiO		Si	SiO	1509.2	Si	SiO		Si	SiO		Si	SiO	1294.1	Si	SiO	2072.5
Si	SiO	727.9	Si	SiO		Si	SiO	754.6	Si	SiO		Si	SiO		Si	SiO	647.1	Si	SiO	104.8
Si	SiO total	2183.7	Si	SiO total	0	Si	SiO total	2263.8	Si	SiO total	0	Si	SiO total	0	Si	SiO total	1941.2	Si	SiO total	2177.3
O	A	10020.1	O	A		O	A	11675.2	O	A		O	A		O	A	7030.2	O	A	12252
O	B	0	O	B		O	B	175.8	O	B		O	B		O	B	3515.1	O	B	114
O	Total	10020.1	O	Total	0	O	Total	11851	O	Total	0	O	Total	0	O	Total	10545.3	O	Total	12366
C	A	2499.4	C	A		C	A	2791.1	C	A		C	A		C	A	4598.7	C	A	1835.4
C	B	763.7	C	B		C	B	483.1	C	B		C	B		C	B	818.6	C	B	752.9
C	C	413.1	C	C		C	C	0	C	C		C	C		C	C	135.7	C	C	352.6
C	Total	3676.2	C	Total	0	C	Total	3274.2	C	Total	0	C	Total	0	C	Total	5553	C	Total	2940.9
AR18			AR19			AR20			AR21			AR22			AR23			AR24		
Nb	A	N/a	Nb	A	468.2	Nb	A	338.7	Nb	A	N/a									
Nb	B	N/a	Nb	B	312.2	Nb	B	225.8	Nb	B	N/a									
Nb	Total	0	Nb	Total	780.4	Nb	Total	564.5	Nb	Total	0									
Si	Si	503.9	Si	Si	1351.9	Si	Si	1061.5	Si	Si	999.9	Si	Si	1844.5	Si	Si	735	Si	Si	32.8
Si	Si	252	Si	Si	675.9	Si	Si	530.7	Si	Si	499.9	Si	Si	922.2	Si	Si	367.5	Si	Si	16.4
Si	Si	0	Si	Si	539.2															
Si	Si	0	Si	Si	269.9															
Si	Si Total	755.9	Si	Si Total	2027.8	Si	Si Total	1592.2	Si	Si Total	1499.8	Si	Si Total	2766.7	Si	Si Total	1102.5	Si	Si Total	858.3
Si	SiO	328.8	Si	SiO	1069.3	Si	SiO	667.4	Si	SiO	1061.5	Si	SiO	615.6	Si	SiO	325	Si	SiO	1221.9
Si	SiO	222.3	Si	SiO	654.9	Si	SiO	554.1	Si	SiO	380.4	Si	SiO	1439.7	Si	SiO	162.5	Si	SiO	610.9
Si	SiO total	551.1	Si	SiO total	1724.2	Si	SiO total	1221.5	Si	SiO total	1441.9	Si	SiO total	2055.3	Si	SiO total	487.5	Si	SiO total	1832.8
O	A	4039	O	A	8790.4	O	A	6941.8	O	A	6710	O	A	10645	O	A	2620.8	O	A	4699.2
O	B	121.7	O	B	0	O	B	0	O	B	0	O	B	750.1	O	B	1237.6	O	B	2337
O	Total	4160.7	O	Total	8790.4	O	Total	6941.8	O	Total	6710	O	Total	11395.1	O	Total	3858.4	O	Total	7036.2
C	A	1059.2	C	A	2650.6	C	A	1496.6	C	A	2939.3	C	A	3148.5	C	A	0	C	A	3485.5
C	B	106	C	B	863.2	C	B	458.5	C	B	0	C	B	0	C	B	1204	C	B	606.4
C	C	0	C	C	0	C	C	228	C	C	185	C	C	19.9	C	C	109.5	C	C	358.8
C	Total	1165.2	C	Total	3513.8	C	Total	2183.1	C	Total	3124.3	C	Total	3168.4	C	Total	1313.5	C	Total	4450.7
AR25			AR26			AR27			AR28			AR29			AR30			AR31		
Nb	A	550.8	Nb	A	336.2	Nb	A	477.2	Nb	A	0									
Nb	B	367.2	Nb	B	224.1	Nb	B	318.1	Nb	B	0									
Nb	Total	918	Nb	Total	560.3	Nb	Total	795.3	Nb	Total	0									
Si	Si	1467.5	Si	Si	920.7	Si	Si	1762.6	Si	Si	1075.5	Si	Si	307.3	Si	Si	829.4	Si	Si	691.2
Si	Si	733.7	Si	Si	460.3	Si	Si	881.3	Si	Si	537.9	Si	Si	153.6	Si	Si	414.7	Si	Si	345.6
Si	Si	0																		
Si	Si	0																		
Si	Si Total	2201.2	Si	Si Total	1381	Si	Si Total	2643.9	Si	Si Total	1613.4	Si	Si Total	460.9	Si	Si Total	1244.1	Si	Si Total	1036.8
Si	SiO	862.7	Si	SiO	493.3	Si	SiO	1464.7	Si	SiO	1640.6	Si	SiO	282	Si	SiO	808.5	Si	SiO	866.7
Si	SiO	1450	Si	SiO	246.7	Si	SiO	732.4	Si	SiO	820.3	Si	SiO	141	Si	SiO	404.2	Si	SiO	433.3
Si	SiO total	2312.7	Si	SiO total	740	Si	SiO total	2197.1	Si	SiO total	2460.9	Si	SiO total	423	Si	SiO total	1212.7	Si	SiO total	1300
O	A	7775.5	O	A	5960.6	O	A	10600.2	O	A	7368	O	A	2376	O	A	5992	O	A	5806.8
O	B	3355.1	O	B	455.6	O	B	0	O	B	2220.3	O	B	342.5	O	B	0	O	B	0
O	Total	11130.6	O	Total	6416.2	O	Total	10600.2	O	Total	9588.3	O	Total	2718.5	O	Total	5992	O	Total	5806.8
C	A	3755.2	C	A	2133.8	C	A	970.4	C	A	3550.9	C	A	998.2	C	A	1792.4	C	A	2419.4
C	B	236.9	C	B	254	C	B	1721.4	C	B	326.7	C	B	20.8	C	B	308.4	C	B	73.5
C	C	281.3	C	C	0	C	C	185.2	C	C	512.9	C	C	270	C	C	0	C	C	143.2
C	Total	4273.4	C	Total	2387.8	C	Total	2877	C	Total	4389.9	C	Total	1289	C	Total	2100.8	C	Total	2636.1

AR32		
Compound	Peak ID	Peak Area
Nb	A	0
Nb	B	0
Nb	Total	0
Si	Si	962.9
Si	Si	481.5
Si	Si	0
Si	Si	0
Si	Si Total	1444.4
Si	SiO	835
Si	SiO	417.5
Si	SiO total	1252.5
O	A	5995.5
O	B	0
O	Total	5995.5
C	A	1833.8
C	B	165.6
C	C	86.7
C	Total	2086.1

Appendix D: Sample Notes

Sample	Notes	Growth?
AR-3	15 min - 15min D1 -> 55 sec, D3 - 55 Seconds Furnace at 150 C 20 CYCLES	
AR-4	15 min - 15min D1 -> 55 sec, D3 - 55 Seconds Furnace at 150 C 20 CYCLES	yes
AR-5	15 min - 15min D1 -> 55 sec, D3 - 55 Seconds Furnace at 150 C 10 CYCLES	yes
AR-6	15 min - 15min D1 -> 55 sec, D3 - 55 Seconds Furnace at 150 C 20 CYCLES New samples, changed pumped oil	yes
AR-7	15 min - 15min D1 -> 55 sec, D3 - 55 Seconds Furnace at 150 C 20 CYCLES IPA wipe	yes
AR-8	15 min - 15min D1 -> 55 sec, D3 - 55 Seconds Furnace at 150 C 20 CYCLES	no
AR-9	15 min - 15min D1 -> 55 sec, D3 - 55 Seconds Furnace at 150 C 20 CYCLES	no
AR-10	15 min - 15min D1 -> 55 sec, D3 - 55 Seconds Furnace at 150 C 20 CYCLES Changed pump oil	no
AR-11	15 min - 15min D1 -> 55 sec, D3 - 55 Seconds Furnace at 150 C 20 CYCLES IPA wipe	no
AR-12	15 min - 15min D1 -> 55 sec, D3 - 55 Seconds Furnace at 150 C 20 CYCLES	no
AR-13	15 min - 15min D1 -> 55 sec, D3 - 55 Seconds Furnace at 150 C 20 CYCLES Changed pump oil, IPA wipe	no
AR-14	15 min - 15min D1 -> 55 sec, D3 - 55 Seconds Furnace at 150 C 20 CYCLES IPA wipe	no
AR-15	15 min - 15min D1 -> 55 sec, D3 - 55 Seconds Furnace at 150 C 30 CYCLES	no
AR-16	30 min - 30min D1 -> 55 sec, D3 - 55 Seconds Furnace at 150 C 20 CYCLES IPA wipe, tube replaced	yes
AR-17	30 min - 30min D1 -> 55 sec, D3 - 55 Seconds Furnace at 150 C 20 CYCLES	yes
AR-18	30 min - 30min D1 -> 55 sec, D3 - 55 Seconds Furnace at 150 C 20 CYCLES Changed Pump Oil	no
AR-19	30 min - 30min D1 -> 55 sec, D3 - 55 Seconds Furnace at 150 C 20 CYCLES	no
AR-20	30 min - 30min D1 -> 55 sec, D3 - 55 Seconds Furnace at 150 C 20 CYCLES	no
AR-21	30 min - 30min D1 -> 55 sec, D3 - 55 Seconds Furnace at 175 C 20 CYCLES tube replaced, IPA wipe	no
AR-22	30 min - 30min D1 -> 55 sec, D3 - 55 Seconds Furnace at 150 C 20 CYCLES	yes
AR-23	30 min - 30min D1 -> 55 sec, D3 - 55 Seconds Furnace at 150 C 20 CYCLES tube replaced	yes
AR-24	30 min - 30min D1 -> 55 sec, D3 - 75 Seconds Furnace at 150 C 20 CYCLES IPA wiped	no
AR-25 and AR-26	30 min - 30min D1 -> 55 sec, D3 - 55 Seconds Furnace at 150 C 20 CYCLES tube replaced, new samples	yes
AR-27 and AR-28	30 min - 30min D1 -> 55 sec, D3 - 55 Seconds Furnace at 150 C 20 CYCLES	yes
AR-29 and AR-30	30 min - 30min D1 -> 55 sec, D3 - 55 Seconds Furnace at 150 C 20 CYCLES Changed Pump oil	no
AR-31	30 min - 30min D1 -> 55 sec, D3 - 55 Seconds Furnace at 150 C 30 cycles	no
AR-32	30 min - 30min D1 -> 55 sec, D3 - 55 Seconds Furnace at 150 C 30 cycles	no
AR-33	30 min - 30min D1 -> 55 sec, D3 - 55 Seconds Furnace at 150 C 30 cycles	?
AR-34	30 min - 30min D1 -> 55 sec, D3 - 55 Seconds Furnace at 150 C 30 cycles New wafers	?

Appendix E: SOP for ALD

In this Appendix, there will be a more procedural SOP for the ALD in the lab. All abbreviations refer to Fig. E.1

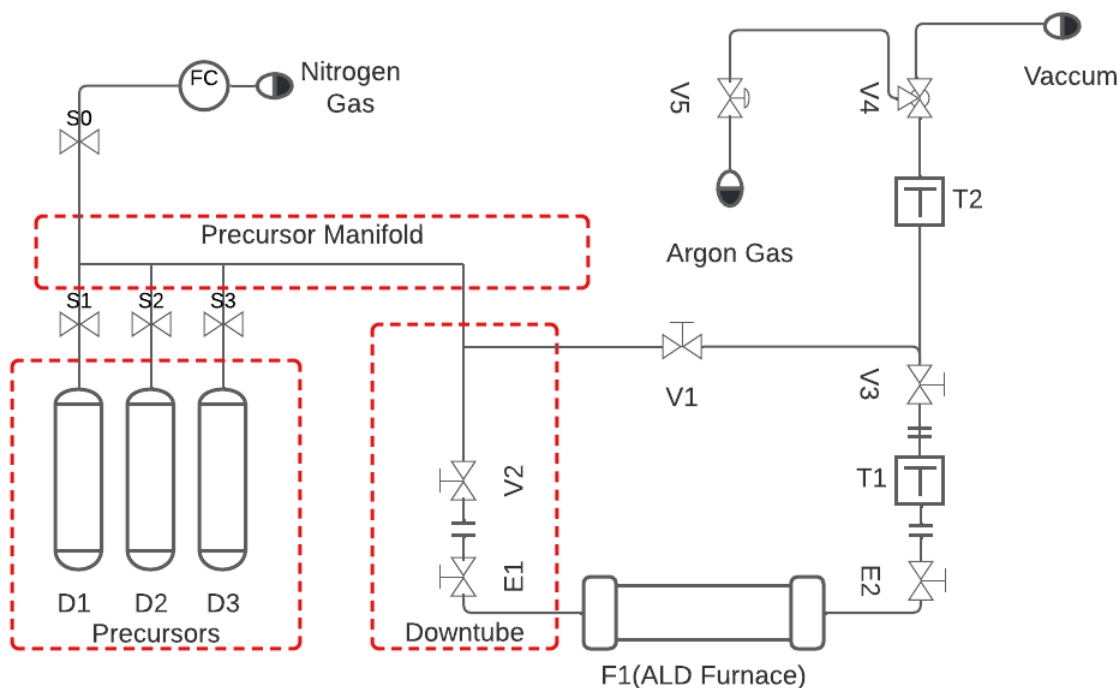


Figure E-1: ALD schematic

Replacing E1:

E1 is attached to the downtube using a silicon tube. Every 5 runs or so, this tube needs to be replaced.

1. Remove the fiber quartz insulation around E1.
2. Remove tin foil and heat tape.
3. Remove silicon tube.
4. Recut tube.
5. Regrease downtube connection and place silicon tube onto connection.
6. Regrease end of elbow E1 and place it on other end of silicon tube.
7. Replace heat tubing and wrap in tin foil to hold in place. **MAKE SURE TINFOIL DOES NOT TOUCH TUBE FURNACE OR IT WILL SHORT.**

8. Wrap fiber quartz around all areas of E1 to ensure proper insulation.

Pre-run:**Prepping E1**

1. Remove stopcock from E1. Wipe with IPA and Kim wipe to remove excess grease.
2. Repeat same step with stopcock joint on E1.
3. Regrease the stopcock joint on E1. Place a sparing amount of grease on your pinky finger and rub around the top of the joint.
4. Regrease the stopcock itself. Place a small amount of grease around the stopcock using your finger
5. Place the stopcock into the joint and turn the stopcock to form a clear seal. Then, replace the spring and spring clip.
6. Wipe the quarter inch end of E1 with IPA to get rid of any residual grease.

Prepping E2

1. Remove stopcock from E2. Wipe with IPA and Kim wipe to remove excess grease.
2. Repeat same step with stopcock joint on E2.
3. Regrease the stopcock joint on E2. Place a sparing amount of grease on your pinky finger and rub around the top of the joint.
4. Regrease the stopcock itself. Place a small amount of grease around the stopcock using your finger
5. Place the stopcock into the joint and turn the stopcock to form a clear seal. Then, replace the spring and spring clip.
6. Wipe the quarter inch end of E2 with IPA to get rid of any residual grease.

Prepping F1

1. Wipe both ends of F1 with IPA to get rid of any residual grease.
2. Grease ¼ inch end of E1 and end of F1. Place a small dab of grease on your finger and rub grease around both ground glass ends of the F1 and E1. Place F1 into E1 and turn F1 for 4-5 rotations, or until the grease forms a clear film. You may place a green clip at the joint to prevent accidental movement if you wish.

Placing the sample

1. Remove a clean wafer sample from where it is being held.

2. Grab wafer with tweezers and careful blow with argon gas.
3. Careful transfer the wafer to F1.
4. Using the spatula, push the wafer towards the center of F1. Place it slightly behind the thermocouple.

Attaching E2

1. Once the wafer is placed in F1, grease the other ground glass end of F1 and the ground glass end of E2.
2. Place E2 into F1 and turn E2 4-5 times, ensuring a good seal is formed as before. When turning, be careful with F1, as it might turn as well as displace the wafer.
3. After turning, ensure the thermocouple touching F1 is still in a good position, and that the wafer is still in the desired spot. If not, remove E2 and adjust.
4. Ensure that the stopcock on E2 is in the closed position before moving onto the next step.

Pulling Vacuum

1. Make sure the stopcocks on E1 and E2 are closed before continuing.
2. Open V2
3. The Mass Flow Controller (MFC) should spike up to around 400 when you open V2. When the MFC reads 40-50 again, you may proceed.
4. Slowly open the stop cock. If it is not opened slowly, then the turbulence created by the vacuum being pulled might displace the wafer.
5. Once the stopcock is open, the pressure will spike to 9999. It should take a minute or two to restabilize to 40-50.

Setting up trap T1

1. Grease the smaller end of E2 and the top end of the trap T1.
2. Take a silicon tube and place it on the end of T1. Slide the end of E2 into the other end of the tube
3. Ensure that the Schlenk line is connected to the other end of T1. If not, place the hose clamp around the joint and tighten with a screwdriver.
4. Open the stopcock valve on E2 to pull a vacuum on T1.
5. The pressure will spike again to 9999 again. It should take a couple minutes to stabilize again.
6. Open V3 and close V2 to complete the loop.

Final set up

1. Place liquid nitrogen in respective containers and place containers around traps.
2. Close tube furnace and tighten chain around it.
3. Place fiber quartz around both openings to ensure proper insulation

Pre – run checklist

- V2 is open
- Stop cocks on E1 and E1 are open
- V3 is open
- V1 is closed
- MFC reads 40-50, record what this pressure is.

Once all these are checked off, ensure the proper running parameters are set in the LabVIEW program and click “Go Recipe”

Mid-Run steps

1. After the initial wait time, top off traps with liquid nitrogen.
2. Record pressure after argon flow starts.
3. For longer runs, top of traps with liquid nitrogen every 30 minutes.

Post- Run steps

1. When run is complete, remove nitrogen containers from the traps
2. Open the furnace. Be careful, as it will be hot.
3. Close V2 and E1 stopcock.
4. Turn V4 to the halfway position, so no line is connected to vacuum.
5. Turn V5 to start Argon flow.
6. Open V4 to the argon line. This will allow for the ALD furnace to be pressurized.
7. After 15-20 seconds, close V4 halfway.
8. Disconnect T1 from E2. If it is still not possible, reopen V4 to pressurize more.
9. Access sample and place where convenient.

Bibliography

1. Energy Production and Consumption - Our World in Data <https://ourworldindata.org/energy-production-consumption>.
2. Why Is Renewable Energy Important? *REN21*, 2019.
3. How Much Fossil Fuel is Left? <https://agesustainability.com/how-much-fossil-fuel-is-left/>.
4. Why Solar Energy Is Important <https://www.empower-solar.com/blog/why-choose-solar-importance-of-solar-energy-empower-solar/>.
5. About Solar Energy <https://www.seia.org/initiatives/about-solar-energy>.
6. Tandem Solar Cells: A Solution to Demand for Renewable Energy <http://large.stanford.edu/courses/2018/ph240/swifter1/>.
7. Carl, A. Soft, Organic, Carrier-Selective Contacts at Inorganic Semiconductor Interfaces Enabled by Low-Defect Covalent Bonding. Ph.D. Dissertation, Worcester Polytechnic Institute, Worcester, MA, 2020.
8. Photovoltaics <https://www.seia.org/initiatives/photovoltaics>.
9. Solar Photovoltaic Cell Basics <https://www.energy.gov/eere/solar/solar-photovoltaic-cell-basics>.
10. How a Solar Cell Works <https://www.acs.org/content/acs/en/education/resources/highschool/chemmatters/past-issues/archive-2013-2014/how-a-solar-cell-works.html>.
11. Applications of Photoelectron Spectroscopy - Chemistry LibreTexts [https://chem.libretexts.org/Bookshelves/Physical_and_Theoretical_Chemistry_Textbook_Maps/Supplemental_Modules_\(Physical_and_Theoretical_Chemistry\)/Spectroscopy/Photoelectron_Spectroscopy/Applications_of_Photoelectron_Spectroscopy](https://chem.libretexts.org/Bookshelves/Physical_and_Theoretical_Chemistry_Textbook_Maps/Supplemental_Modules_(Physical_and_Theoretical_Chemistry)/Spectroscopy/Photoelectron_Spectroscopy/Applications_of_Photoelectron_Spectroscopy)
12. 3.1.2 Applications of Thin Films https://www.tf.uni-kiel.de/matwis/amat/semitech_en/kap_3/backbone/r3_1_2.html.
13. What Is Thin Film Deposition? <http://www.semicore.com/news/81-what-is-thin-film-deposition>
14. Thin Films/Properties and Applications | IntechOpen <https://www.intechopen.com/chapters/75002>
15. Short-Range Order - an overview | ScienceDirect Topics <https://www.sciencedirect.com/topics/materials-science/short-range-order>
16. What is a Grain Boundary? - Definition from Corrosionpedia <http://www.corrosionpedia.com/definition/599/grain-boundary-gb>
17. Amorphous Thin Films <https://sites.slac.stanford.edu/stongroup/about-us/research/amorphous-thin-films>.
18. Mean Free Path - an overview | ScienceDirect Topics <https://www.sciencedirect.com/topics/physics-and-astronomy/mean-free-path>.
19. Thin Film Solar Cell, Description and Types <https://solar-energy.technology/photovoltaics/elements/photovoltaic-panel/photovoltaic-cell/thin-film-solar-cell>

20. Atomic Layer Deposition - ScienceDirect
<https://www.sciencedirect.com/science/article/pii/B9780815520313000089>
21. Miikkulainen, V.; Väyrynen, K.; Kilpi, V.; Han, Z.; Vehkamäki, M.; Mizohata, K.; Räisänen, J.; Ritala, M. (Invited) Photo-Assisted ALD: Process Development and Application Perspectives. *ECS Trans.* **2017**, *80* (3), 49–60. <https://doi.org/10.1149/08003.0049ecst>.
22. Page Title <http://www.cabuk1.co.uk/>.
23. Atomic layer deposition enabling higher efficiency solar cells: A review - ScienceDirect
<https://www.sciencedirect.com/science/article/pii/S2589965119300662>.
24. Perovskite Solar | Perovskite-Info <https://www.perovskite-info.com/perovskite-solar>.
25. What is a Perovskite material? | Perovskite-Info <https://www.perovskite-info.com/introduction-perovskites>.
26. Frontiers | Exploring the Properties of Niobium Oxide Films for Electron Transport Layers in Perovskite Solar Cells | Chemistry
<https://www.frontiersin.org/articles/10.3389/fchem.2019.00050/full>.
27. Evaluation and Comparison of Novel Precursors for Atomic Layer Deposition of Nb₂O₅ Thin Films | Chemistry of Materials <https://pubs.acs.org/doi/10.1021/cm2026812>.
28. XPS and UPS Background – Grimmgroup Research.
29. X-ray Photoelectron Spectroscopy https://serc.carleton.edu/msu_nanotech/methods/xps.html.
30. Mendes, J. Interfacial States, Energetics, and Passivation of Large-Grain and Thin-Film Antifluorite Cesium Titanium Bromide. Bachelors Major Qualifying Project, Worcester Polytechnic Institute, Worcester, MA, 2021
31. Dawley, R. Elucidating Surface Sites and Reactivity of a Zirconium-Based MOF Towards Future Capping and Trapping of Guest Molecules. Bachelors Major Qualifying Project, Worcester Polytechnic Institute, Worcester, MA, 2021
32. Materials Data on Si by Materials Project, 2020. <https://doi.org/10.17188/1190959>.
33. Materials Data on Nb₂O₅ by Materials Project, 2020. <https://doi.org/10.17188/1276924>.
34. Daccà, A.; Gemme, G.; Genova, I. XPS Characterization of Niobium for RF Cavities. **1997**, 18.
35. Effective passivation of silicon surfaces by ultrathin atomic-layer deposited niobium oxide: Applied Physics Letters: Vol 112, No 24 <https://aip.scitation.org/doi/10.1063/1.5029346>.